

# **Parametric Modeling Program of Fillet End Mill**

**Jiapu Zhu**

A Thesis

In the Department

of

Mechanical and Industrial Engineering

Presented in Partial Fulfillment of the Requirements

For the Degree of Master of Applied Science at

Concordia University

Montreal, Quebec, Canada

March 2016

© Jiapu Zhu, 2016

# CONCORDIA UNIVERSITY

## School of Graduate Studies

This is to certify that the thesis prepared

By: Jiapu Zhu

Entitled: Parametric Modeling Program of Fillet End Mill and submitted in partial fulfillment of the requirements for the degree of

### Master of Applied Science

Complies with the regulations of the University and meets the accepted standards with respect to originality and quality.

Signed by the final examining committee:

Dr. Brandon W. Gordon Chair

Dr. Wenfang Xie Examiner

Dr. Zhenhua Zhu Examiner

Dr. Z. C. Chen Supervisor

Approved by \_\_\_\_\_

Chair of Department or Graduate Program Director

\_\_\_\_\_

Dean of Faculty

Date \_\_\_\_\_

# ABSTRACT

Parametric Modeling Program of Fillet End Mill

Jiapu Zhu

End-mill cutter is the most commonly used cutting tool in metal machining industry, especially flat end-mill and fillet end-mill, which provide significant influence on machining efficiency and quality.

Nickel-based high temperature alloy is widely used in aerospace industry due to its excellent performance of mechanical property under rigorous situation. However, it possesses poor machinability and requires very high cutting force during milling process. In addition, vibration is another factor which should be taken into consideration.

Variable pitch end-mill is one kind of end-mill cutters that have different parameters in pitch and flute. In this category of design, each integrated cutting feature, namely, bottom, fillet, side, flute and gash are different. Meanwhile, it also can reduce the vibration effectively.

FEA simulation is a time saving and cost saving way in the field of cutting tool design and optimization. An efficient and accurate modeling method is demanded due to the complexity geometry of end-mill cutter.

A lot of research was conducted on end-mill modeling previously. However, most of them focused on symmetric geometry end-mill and there were no introduction about gash modeling. Based on the above reasons, a feature-based modeling method with parametric design is proposed. According to the

characteristic of end-mill and based on the mathematic Equations, each feature is designed and modeled individually. Constraints of gash are analyzed and applied. In addition, a customized program is developed with the combination of Visual Basic user interface and CATIA macro programing technique. Finally, a simulation example of the model is conducted to analyze the dynamics during cutting process.

## **ACKNOWLEDGEMENTS**

I hereby would like to express my sincere gratitude to my supervisor, Dr. Chevy Chen, for his kind guidance, patient instructions and constant encouragement through all this work. It benefits me quite a lot going through all this research, I would not accomplish thesis without him.

Additionally, I would like to say thanks to all my dear colleagues in our lab, for every generous help from everyone when I encountered any problems.

Finally, I give my special thanks to my parents and girlfriend, for all their endless love and continuous support in every aspect all through these years.

# TABLE OF CONTENTS

- LIST OF FIGURES..... viii
- LIST OF TABLES..... xi
- CHAPTER 1 INTRODUCTION..... 1
  - 1.1 Nickel-based high-temperature alloy..... 1
  - 1.2 End-mill..... 2
  - 1.3 Feature-based Design and Parametric Design ..... 4
  - 1.4 CATIA-Based Macro Programming Technique with Visual Basic Script..... 5
  - 1.5 Literature Review..... 6
  - 1.6 Objective of Thesis..... 7
  - 1.7 Thesis Outline ..... 9
- CHAPTER 2 FEATURE MODELING OF THE END-MILL CUTTER..... 10
  - 2.1 Basics of the End-Mill Cutter ..... 10
  - 2.2 Feature Modeling of the End-mill Cutter ..... 11
    - 2.2.1 Toolbar..... 11
    - 2.2.2 Flute..... 14
    - 2.2.3 Bottom cutting edge..... 15
    - 2.2.3 Side cutting edge..... 23
    - 2.2.4 Fillet..... 26
- CHAPTER 3 FEATURE MODELING OF GASH..... 32
  - 3.1 Introduction ..... 32
  - 3.2 Guide direction ..... 37
  - 3.3 Gash profile..... 42

CHAPTER 4 PARAMETRIC MODELING PROGRAM OF END MILL ..... 56

    4.1 Customized Modeling Program ..... 56

    4.2 Verification of the Modeling Program..... 57

CHAPTER 5 APPLICATION ..... 70

    5.1 Introduction ..... 70

    5.2 Settings of Simulation Software ..... 70

CHAPTER 6 CONCLUSIONS AND FUTURE WORK..... 76

    6.1 Conclusions..... 76

    6.2 Future Work..... 77

BIBLIOGRAPHY ..... 78

# LIST OF FIGURES

Figure 1.1 Engine of rocket..... 2

Figure 1.2 Different Types of End-mill Cutters..... 3

Figure 1.3 Chipping of the edge on a flat end-mill..... 4

Figure 2.1 Illustration of end-mill..... 11

Figure 2.2 Annular surface of radius corner..... 13

Figure 2.3 Toolbar of fillet end-mill..... 13

Figure 2.4 Flute..... 14

Figure 2.5 Orthogonal model ..... 16

Figure 2.6 Terms used in metal cutting..... 16

Figure 2.7 The exterior endpoint of bottom cutting edge ..... 18

Figure 2.8 Bottom edge structure ..... 19

Figure 2.9 The definition of  $\theta$  ..... 21

Figure 2.10 Orthogonal model of bottom clearance face ..... 22

Figure 2.11 Clearance profile..... 23

Figure 2.12 Connection of fillet and side edge..... 24

Figure 2.13 Start point on annular surface..... 25

Figure 2.14 Side edge clearance face ..... 26

Figure 2.15 Fillet flank ..... 27

Figure 2.16 Boundary curves..... 28

Figure 2.17 Intersection between bottom and side flank..... 29

Figure 2.18 Fillet cutting edge ..... 30

Figure 2.19 Connect curve.....	31
Figure 2.20 Fill surface function .....	31
Figure 3.1 Gash .....	32
Figure 3.2 Gash comparison .....	33
Figure 3.3 Gash machining process.....	33
Figure 3.4 Parameter illustration.....	35
Figure 3.5 Gash profile.....	36
Figure 3.6 Gash comparison .....	36
Figure 3.7 Guide direction .....	37
Figure 3.8 Vertical plane.....	38
Figure 3.9 Rake face.....	39
Figure 3.10 Cone property.....	41
Figure 3.11 Guide line.....	42
Figure 3.12 Coordinate of black point.....	43
Figure 3.13 Intersection side line .....	46
Figure 3.14 Second side line.....	47
Figure 3.15 Constraint line of gash bottom.....	49
Figure 3.16 Intersection line position.....	50
Figure 3.17 Gash profile.....	53
Figure 3.18 Gash surface .....	54
Figure 3.19 Final model of end mill .....	55
Figure 4.1 User face of program.....	57
Figure 4.2 Toolbar parameters.....	63
Figure 4.3 Flute parameters .....	64
Figure 4.5 Side edge parameters.....	67

Figure 4.6 Gash parameters ..... 68

Figure 5.1 Project setting..... 71

Figure 5.2 Cutting tool and work piece setting ..... 72

Figure 5.3 Redrawn model ..... 73

Figure 5.4 Parameters of cutting process..... 74

Figure 5.5 Simulation result..... 75

# LIST OF TABLES

Table 2.1 Parameters of toolbar..... 12

Table2.2 Flute parameters ..... 15

Table 2.2 Parameters of bottom cutting edge ..... 17

Table2.3 Design parameters of side cutting edge..... 25

Table 3.1 Design parameters of gash1 ..... 34

Table 4.1 Parameters of cutter STR440M ..... 57

# CHAPTER 1 INTRODUCTION

## 1.1 Nickel-based high-temperature alloy

Due to the excellent performance of mechanical property, thermal stability, oxidation resistance and high temperature deformation resistance, high-temperature alloy is widely used as the material on the component that work under rigorous conditions.

To be classified by base material, there are three different kinds of high-temperature alloys, nickel-based, iron-based and cobalt-based. Comparing all these three high-temperature alloys, iron-based alloy costs less, but its mechanical performance is poorer than the other two materials; Cobalt-based alloy provides a relatively high mechanical property but the cost is much higher than the others; Nickel-based alloy could guarantee good mechanical performance and the cost is acceptable at the same time. Therefore, nickel-based alloy is widely used in mechanical industry. Currently, more than 60% of nickel-based alloy is utilized in aerospace industry, especially as the material for the engine on the rocket.

However, as the result of high hardness, high strength and low plasticity, nickel-based high-temperature alloy possesses poor machinability. Hence, the machining process is the key to the application of nickel-based high-temperature alloy.



**Figure 1.1 Engine of rocket**

## **1.2 End-mill**

Milling is one of the most popular machining processes and has been extensively applied in metal machining. With the development of manufacture industry, more and more difficult-to-cut material are widespread. Since the demand for precision and complexity of the work piece is raised up and new CNC machines have been applied, the requirements for end-mill are increased as well. To satisfy the requirement of industry, the material and shape of end-mill grows rapidly that lead to a complicated catalog of end-mill. To be classified by geometry, there are end-mills like flat end-mill (flat nose), ball end-mill (ball nose), fillet end-mill (bull nose) and chamfer end-mill, as shown in Figure 1.2.

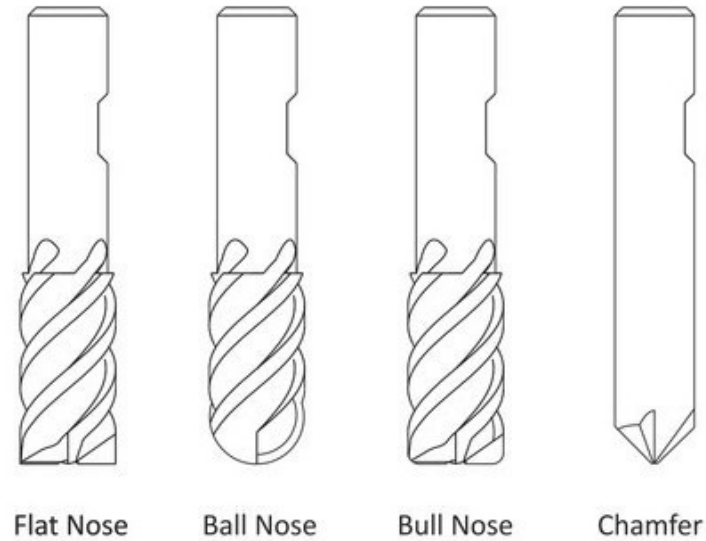


**Figure 1.2 Different Types of End-mill Cutters**

Flat end-mill is normally used to mill flat face and slot. The weakest point of a flat end-mill is the sharp corner which causes chipping or crumbling at cutting edges, as shown in Figure 1.3. Vibration occurs quite often during milling process. Due to this reason, flat end-mill is applied for rough milling. With the continuous cutting edge from the bottom to the end, ball end-mill could avoid vibration effectively during cutting process. Thereby, it could be used for slope milling and surface finishing. Fillet end-mill possesses flat end with corner radius which provides a higher strength and stronger rigidity when compared with the other two categories of end-mills. Fillet end-mill is usually utilized in machining of difficult-to-cut material, high speed machining and high feed rate machining. This thesis mainly focus on flat end-mill and fillet end-mill.



**Figure 1.3 Chipping of the edge on a flat end-mill**

End-mill is generally manufactured using CNC grinding machine through the specific CAM software in industry. Based on processing sequence, there are four main features that consist of milling cutter, which are flute, gash, bottom edge and side edge. The space of flute and gash affect chip evacuation and dynamic performance. The geometry of both bottom and side cutting edge affects the product's service time and cutting performance. Due to some values of the parameters of the features are small, even little change may have greatly influence to cutting performance. Only well-designed features will achieve better performance and a precise model will delivery good simulation result.

### **1.3 Feature-based Design and Parametric Design**

A product model can be built by using (design) features, which known as design by features

or feature based modeling. Features can be seen as package of information which contains different forms and attributes of a part, this information can be used to explain the design, part manufacture or assemblies which they are related to [1]. Comparing to traditional design, feature-based design has a clear structure, which is helpful to the designer from the top view. Meanwhile, each feature which integrates all the corresponding parameters, dimensions and constraints are specified with relations.

Now, one of the core techniques of CAD is parametric part modeling. Since the functions of parametric modeling in major commercial CAD software are introduced, parametric models can be easily built and modified in the design process. The parametric representation of features provides a powerful way to change features with respect to their dimension. [1] The combination of feature-based design and parametric design brings a direct view of the product to the designer. Even the unprofessional person could have a comprehensive understanding with a developed feature-based model.

## **1.4 CATIA-Based Macro Programming Technique with Visual Basic Script**

CATIA (Computer-graphics Aided Three-dimensional Interactive Application), is an integrated 3D CAD/CAE/CAM software that is developed by Dassault System Company, which locates in France, in 1975. CATIA is the software that can be applied on the design of a product from the start to the end, which means it covers concept design, industry design, 3D modeling design, analysis, dynamic calculation, simulation, drafting and manufacturing. CATIA is able to provide multi- functional module that includes Part Design, Assembly Design and Interactive Drafting etc. This thesis mainly focus on Part Design and Generative Shape Design. Macro

programming is a powerful function in CATIA which records almost all the steps while using CATIA. By applying the parameters into the script, the parametric model is easily to be obtained.

Visual Basic (VB) is a high-level programming language and is designed to be an approachable and easy-to-learn language. It is widely used due to its easy-to-use, universal and high efficiency features. With the visual studio platform, feature-based design and parametric design can be applied perfectly by using its friendly interface. In addition to the important points mentioned above, CATIA provides corresponding components which is able to be added to the application as references so that the users could call functional module of CATIA via VB script.

## **1.5 Literature Review**

Many research have conducted and the end-mill models were proposed. Tandon and Khan [2] use three dimensional parameters to describe in detail the methodology to model the geometry of a flat end mill. They also used the modeled tool for finite element simulations to study the cutting flutes under static and transient dynamics load condition. Kim and Park [3] propose a method that by using cutting process simulation, the machined shape of end mill is obtained by using Boolean operation between a given grinding wheel and a cylindrical work piece. Xu and Zhao [4] combine design and manufacturing process of end mill. An accurate parametric end mill geometric model based on the end mill geometric parameters is proposed and the position of the grinding wheel is calculated. Ren and Tang [5] present a general geometrical models of the cutting edge and groove section of a helical end mill with constant pitch. The section profile and relative feeding speeds of the grinding wheel used in 2-axis NC machining of the end mill are deduced. Pham and Ko [6] also used the groove profile to build the model. The helical groove profile is precisely calculated using a

given wheel profile and the relative movements between the work piece and the grinding wheel. Engin and Altintas [7] proposed a generalized mathematical model of helical end mill. The coordinates of the cutting edge points are mathematically expressed. Altintas, Engin and Budak [8] presented an analytical prediction of stability lobes for milling cutters with variable pitch angles. The solution can be used for optimization design of tooth spacing. Zhao et Al. [9] presented a mathematical model of the relief surface curve which is verified on a five-axis CNC grinding machine. With the model of a cup wheel edge, the coordinates of grinding point and other necessary data, the NC code can be generated for 3D simulation and actual machining with good product. Zhao, Shi and He [10] established the mathematic Equation of rake face based on the fillet of grinding wheel. And the Equation is verified by comparing with the discrete entity of rake face with Boolean operation. Özel [11] proposed a method that by combining modeling of cutting tool and simulation of cutting process, the cutting tool design can be improved and an optimum condition is selected. Kaldor S, Rafael A M. and Messinger D [13] discussed two basic geometric problems in the flute-grinding processes. First problem is the determination of the resulting flute profile for a given grinding wheel cross-section. Second problem is the determination of the wheel profile for a desired flute cross-section. Following the above research, Ehmann [14] developed a program and presented a well solution for the second problem. Kang [15, 16] gave a series papers on the detail calculation of the grinding processes base on the kinematics of grinding processes via CAD approach. Kim and Ko [17] proposed a manufacturing model of flute-grinding processes and gave the mathematical expression of the flute cross-section curve based on the envelope theory.

## **1.6 Objective of Thesis**

Nickel-based high-temperature alloy is widely used in aerospace industry with its good

performance under tough condition. However, the feature of nickel-based high-temperature alloy makes it difficult to be machined and vibration is a common issue. To solve this problem, a variable pitch design is introduced. FEA simulation is a time saving and cost saving method in design and optimization field. However, the industry of cutting tool design, manufacturing and the commercial CAM software does not currently open this function to users which makes it difficult to design new customized cutting tool. Even though many research activities have been conducted, they mainly focused on design of flute. Some of the researches used grinding wheel path to build the model, but the surface is not smooth enough.

In this thesis, an integrated modeling method based on the advanced variable pitch end-mill is proposed. The parameters measured from real cutter have been applied to build the model. Based on the machining process, flute is generated by using flute profile which is accurate and smooth. Then, orthogonal cutting model is introduced. By analyzing the geometry of bottom and side edge, with the design parameters, orthogonal model is applied to develop the clearance face for bottom edge and side edge. Due to the missing theory of fillet design, a relatively smooth fillet flank is derived and the fillet edge is guaranteed. An accurate gash is reached with the analysis of design parameters. Since it is time consuming to build the complex model in CAD software, a program is developed with the combination of Visual Basic interface and CATIA macro programming technique. In addition, by using parametric program, a model is created using the parameters that measured from real end mill cutter and is verified in CATIA. At the end, a FEA simulation is conducted on model under given machining situation. The analysis of result provides suggestion of cutting tool optimization.

## 1.7 Thesis Outline

This thesis consists of six chapters. Chapter 1 introduces commonly used material and cutting tool. Then, feature-based design and parametric design is discussed. After that, a widely used CAD software and a simple programming language are presented. At last, literatures are reviewed about this topic. Chapter 2 shows the basics of end-mill, followed with the modeling of flute. Orthogonal cutting theory is applied to derive the clearance face of bottom edge and side edge. At the end of the chapter, a smooth fillet flank is built. In chapter 3, geometry of gash is discussed and the modeling approach is proposed. With the modeling method, the accurate gash is reached. Chapter 4 shows the developed modeling program first. Then, an example end mill model with parameters measured from a real end mill cutter is generated. Finally, dimensions of the model is measured in CATIA. In chapter 5, a FEA simulation is conducted using Thirdwave Advantedge software. The simulation result is analyzed and an optimization method is developed. Chapter 6 concludes the modeling method of variable pitch end-mill and future work is proposed.

# CHAPTER 2 FEATURE MODELING OF THE END-MILL CUTTER

## 2.1 Basics of the End-Mill Cutter

The end-mill cutter is a milling tool which possesses a complex geometric structure. It is manufactured by a high speed rotating grinding wheel that go through a specific path. This process is controlled by specific commercial CAM software that assorted with the CNC grinding machine. Generally, end-mill cutter has been grinded by CNC machine following particular steps. In this thesis, features will be illustrated following its manufacturing order as well.

In Figure 2.1, it shows the basics of the features of the end-mill cutter.

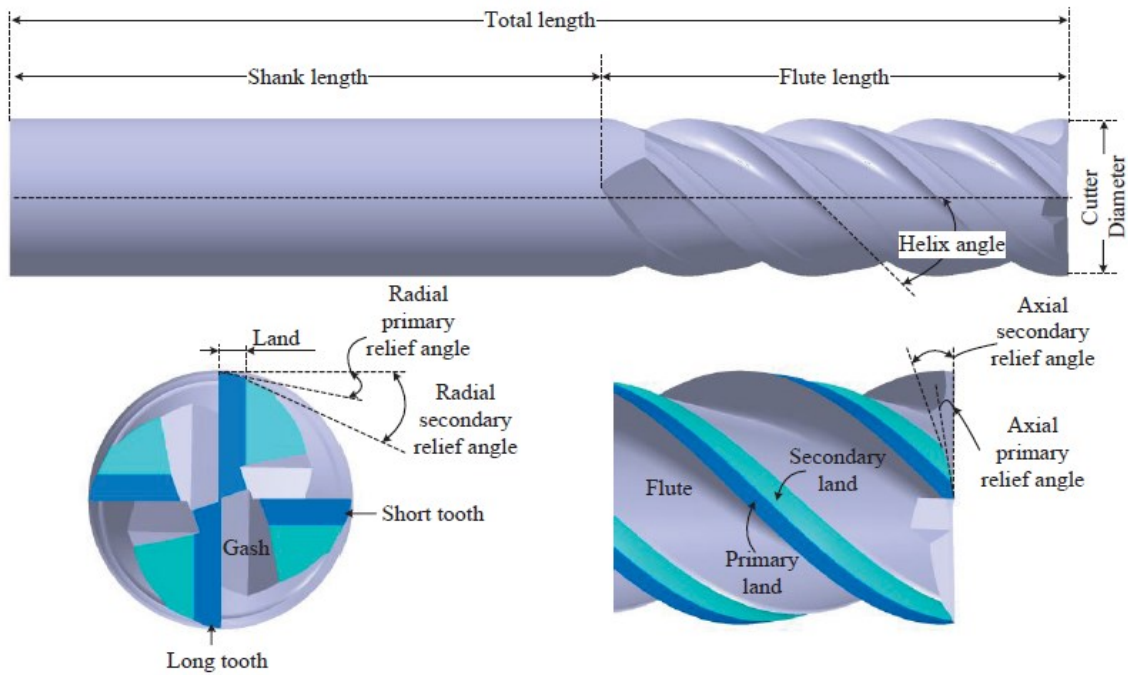


Figure 2.1 Illustration of end-mill

## 2.2 Feature Modeling of the End-mill Cutter

### 2.2.1 Toolbar

Toolbar is the most basic part of an end-mill cutter which includes two parts: shank and flute. However, comparing with flat end-mill cutter, fillet end-mill cutter has one more feature which is corner fillet. Even though there should be a specific and standard connection on the shank part, the modeling of this feature is not included in this thesis. Currently in industry, toolbar is

customized by considering cutting process and has been bought from suppliers. Toolbar can be made from different materials, such as high speed steel, carbide, ceramic and diamond. Carbide is the most commonly used one. Coating technique has also been applied on the toolbar to reduce friction and tool wear phoneme. According to the work piece material and machining requirement, the customized toolbar with particular material, dimension and coating will be bought from suppliers.

For toolbar, the design parameters are shown in Table2.1

**Table 2.1 Parameters of toolbar**

Parameters	Definition	Value
L	Length of the bar	63mm
D	Diameter of the bar	9.978mm
R <sub>c</sub>	Radius of the corner(fillet end-mill only)	0.502mm

For the flat end-mill, the value of R<sub>c</sub> is 0, so that the toolbar of flat end-mill is a cylinder, which is easy to build in CATIA. While the corner with radius is a 1/4 arc, which is tangent with two planes machined by the bottom edge and the side edge as shown in Figure 2.2.To reach the toolbar for the fillet end-mill, a parametric Equation for the annular surface is represented in Eq2.1:

$$S_{corner}(\mu, \delta) = \begin{cases} (\frac{D}{2} - R_c + R_c * \cos \delta) * \cos \mu \\ (\frac{D}{2} - R_c + R_c * \cos \delta) * \sin \mu \\ R_c - R_c * \sin \delta \end{cases} \quad \text{Eq2.1}$$

where, D is the diameter of the bar, R<sub>c</sub> is the radius of the corner and

$$\delta \in \left[0, \frac{\pi}{2}\right]$$

$$\mu \in [0, 2\pi]$$

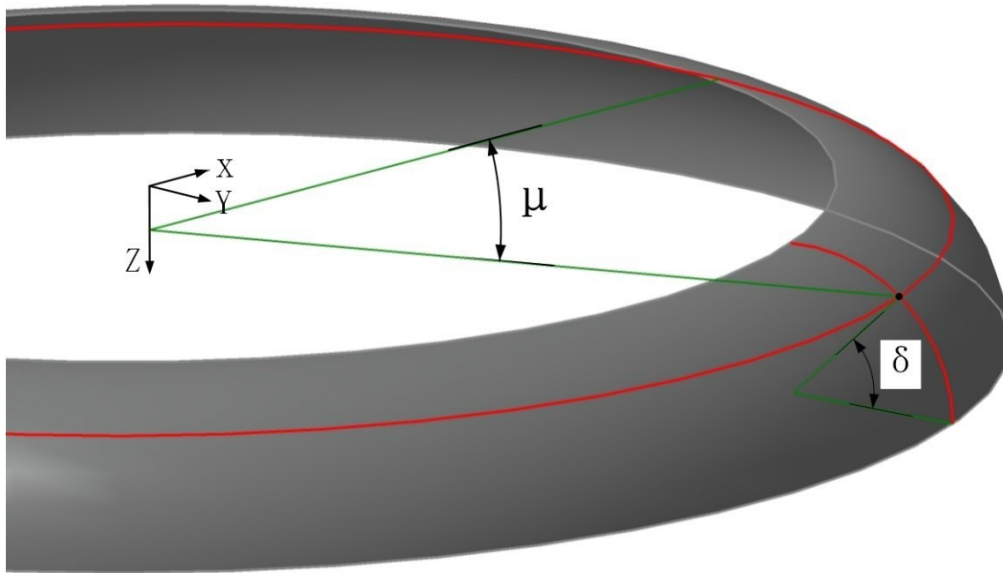


**Figure 2.2 Annular surface of radius corner**

With Eq2.1, by substituting appropriate value of the parameters, the annular surface can be derived using function from CATIA. In order to get the toolbar of fillet end-mill, the boolean operation has been applied to trim the cylinder using the annular surface, as shown in Figure 2.3

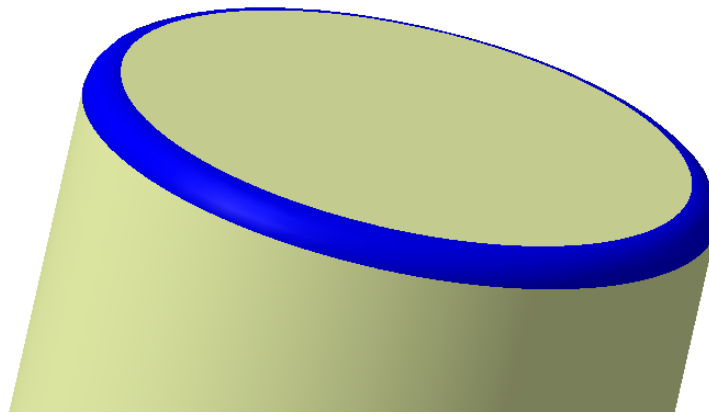


**Figure 2.3 Toolbar of fillet end-mill**

## 2.2.2 Flute

Flute is an important feature of the milling cutters, which forms many important tool parameters in the flute structures including rake angle, relief angle, core radius, pitch angle and helix angle. Many researches have been done on this part. A flute profile model [12] is used to build this feature. With this method, the points of the flute profile are inputted and the profile is generated using spline function. Then, a helix line which starts from the first point of the flute profile is developed. Finally, the flute surface is built by sweeping flute profile along helix line, as shown in Figure 2.4.

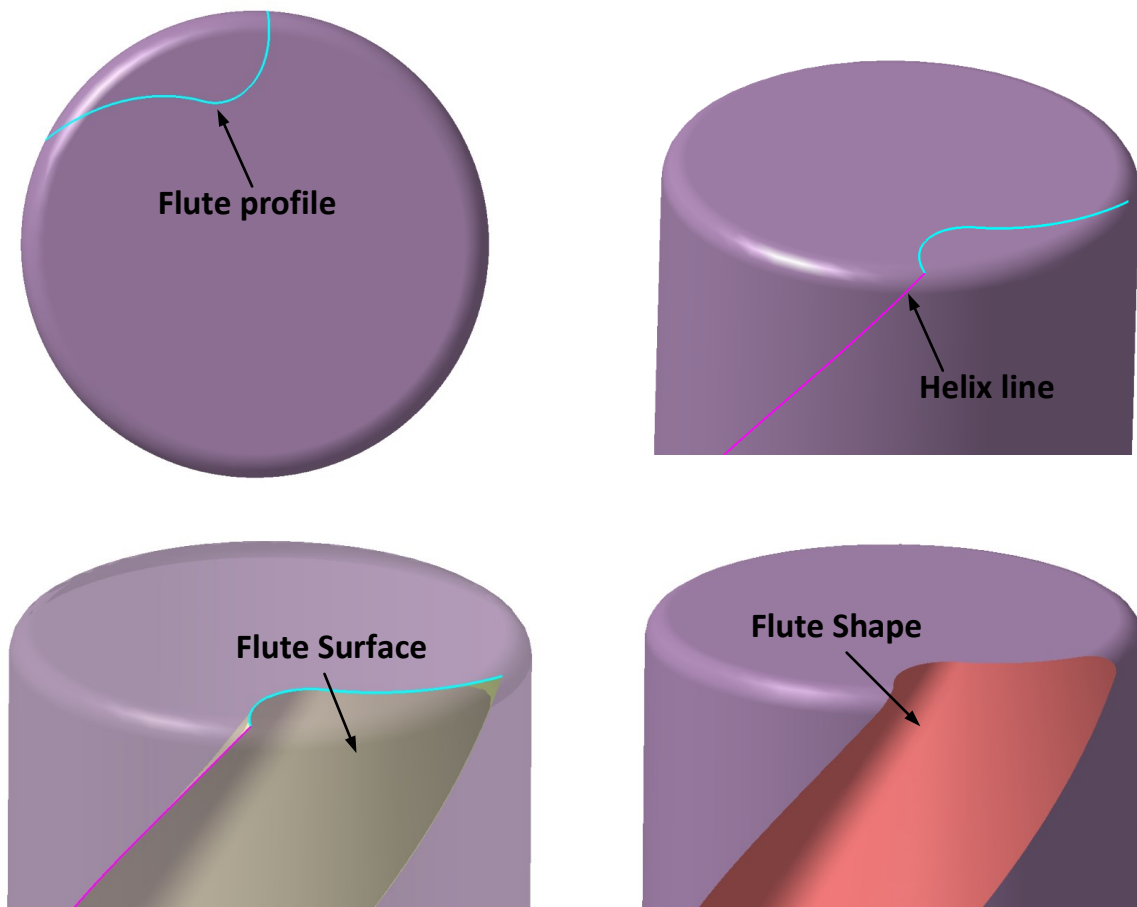


Figure 2.4 Flute

The flute design parameters are listed in Table2.2.

**Table2.2 Flute parameters**

Parameters	Definition	Value
$\alpha_{\text{fluteangle}}$	Pitch angle of the flute	81.5°
$L_{\text{flutelength}}$	Length of the flute	13.5mm
$\beta_{\text{helix}}$	Helix angle of flute	41°

### 2.2.3 Bottom cutting edge

The bottom cutting edge is one of the crucial parameters which will greatly affect the quality of the work piece surface in the milling process. The strength of the bottom cutting edge is the main factor to judge the design of a cutting tool. An end-mill cutter with a good design of the bottom cutting edge not only provides a good performance in the milling process, but also leads a durable tooling service time. Since the variable pitch structure has been applied on the design of end-mill cutter, a complete view of bottom cutting edge is needed. Because the parameters of the bottom cutting edge are defined on the orthogonal plane, the orthogonal cutting will be discussed first.

The mechanics of all metal-cutting process can be simplified as the mode shown in Figure 2.4. The tool is wedge-shaped and has a straight cutting edge. It is constrained to move relatively to the work piece in such a way that a layer of metal is removed in the form of a chip. The cutting edge of the tool is arranged to be perpendicular to the direction of relative work-tool motion,

which is known as orthogonal cutting.

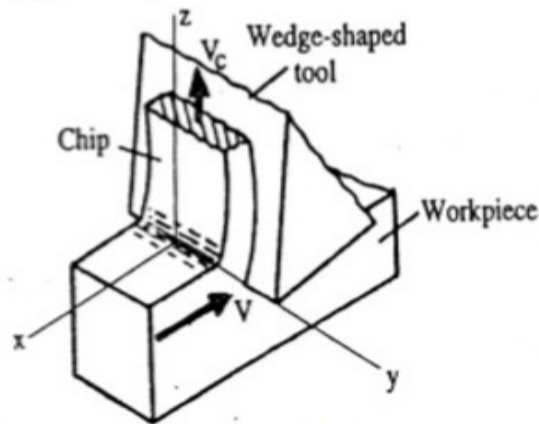


Figure 2.5 Orthogonal model

The wedge-shaped cutting tool basically consists of two surfaces which intersect to form the cutting edge, shown in Figure 2.5. The surface along which the chip flows is known as the rake face, or more simply as the rake, and that surface ground back to clear the new or machined work piece surface is known as the flank.

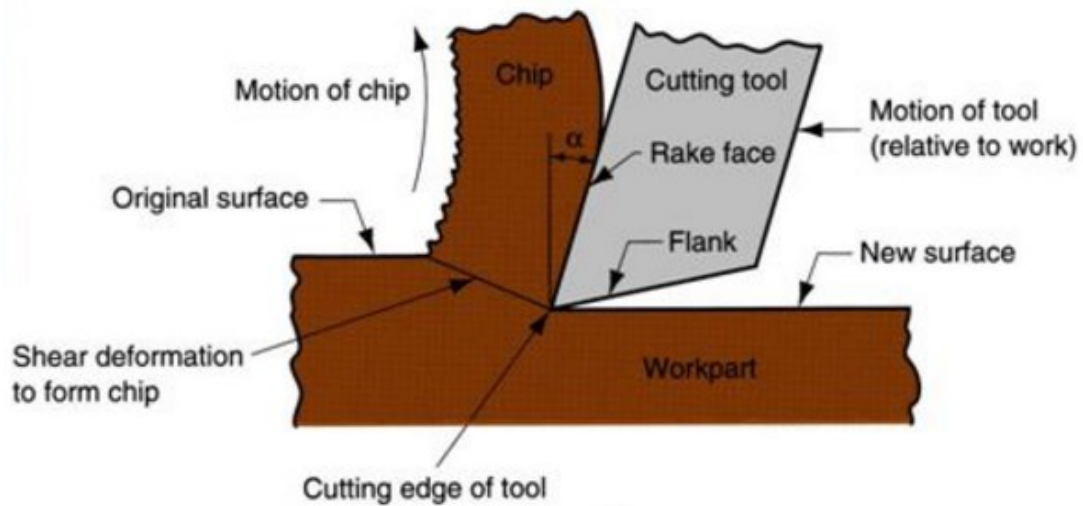


Figure 2.6 Terms used in metal cutting

From the bottom view of the cutter, the geometrical structure of the cutting edges are clearly shown in Figure 2.1. As mentioned before, the bottom edge is made of rake face, flank face and cutting edge. Since the rake face is one part of the gash, so the modeling of it will be illustrated in the gash modeling chapter.

The tool flank plays no part in the process of chip removal; however, the angle between the flank and the new work piece surface can significantly affect the rate at which the cutting tool wears and is defined as the clearance angle or, more precisely, the working normal clearance. If the clearance angle is too small, the tool wear appears rapidly and the tool life is shorten . If the clearance angle is too large, it will weaken the cutting edge. Generally in the design of the end-mill cutter, there will be a secondary flank face and even a tertiary flank face which can lead to a smooth evacuation of the chips.

The intersection of rake face and primary flank face is the cutting edge. It is the first element that should be defined in the bottom cutting edge modeling. With a fixed cutting edge, the other relative element can be found. The design parameters are shown in Table 2.2

**Table 2.2 Parameters of bottom cutting edge**

<b>Parameters</b>	<b>Definition</b>	<b>Value</b>
$\alpha_l$	The angle between the cutting edge and XY plane	1.8°
$D_{\text{radialoffset}}$	The distance between cutting edge and parallel radius line	0.1mm
$D_{\text{axialoffset}}$	The distance between the end point of the cutting edge, which is close to the axis of the cutter, and the axis of the cutter(for long cutting edge, the value is 0)	2.42mm

$\alpha_{\text{rake}}$	The rake angle of cutting edge	$5.5^\circ$
$\alpha_{\text{relief1}}$	The relief angle of first flank	$10^\circ$
$\alpha_{\text{relief2}}$	The relief angle of second flank	$24^\circ$
$\alpha_{\text{relief3}}$	The relief angle of third flank	$30^\circ$
$W_{\text{relief1}}$	Clearance width of the first flank	0.85mm
$W_{\text{relief2}}$	Clearance width of the second flank	1.2mm
$W_{\text{relief3}}$	Clearance width of the third flank	3mm

After the flute profile has been generated, the coordinate of exterior endpoint of bottom cutting edge is derived, as shown in Figure 2.7.

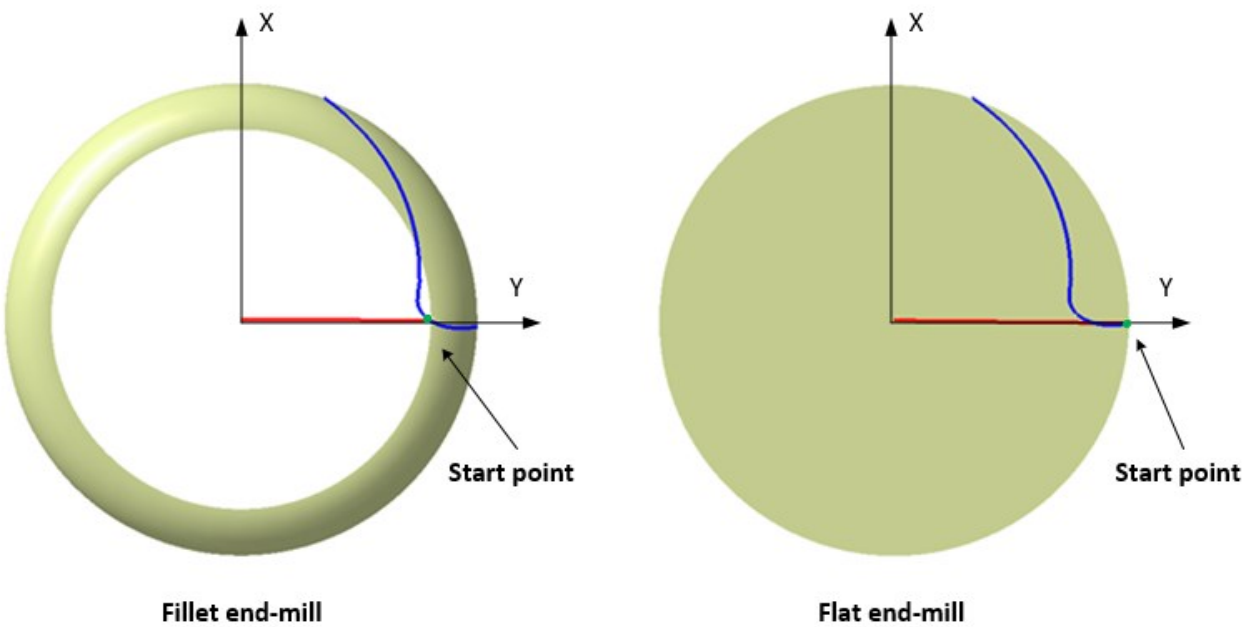


**Figure 2.7 The exterior endpoint of bottom cutting edge**

By connecting the origin point and the endpoint, the parametric Equation of the red line, which is the early form of bottom cutting edge, is represented in Eq2.2

$$P_{edge} = \begin{bmatrix} 0 \\ l \\ 0 \end{bmatrix} \quad \text{Eq2.2}$$

where, D is the diameter of the bar,  $R_c$  is the corner radius and

$$l \in \left[ 0, \frac{D}{2} - R_c \right]$$

To ensure the concavity structure and radial offset, shown in Figure 2.8, the mapping method is applied here to derive the parametric Equation of bottom cutting edge.

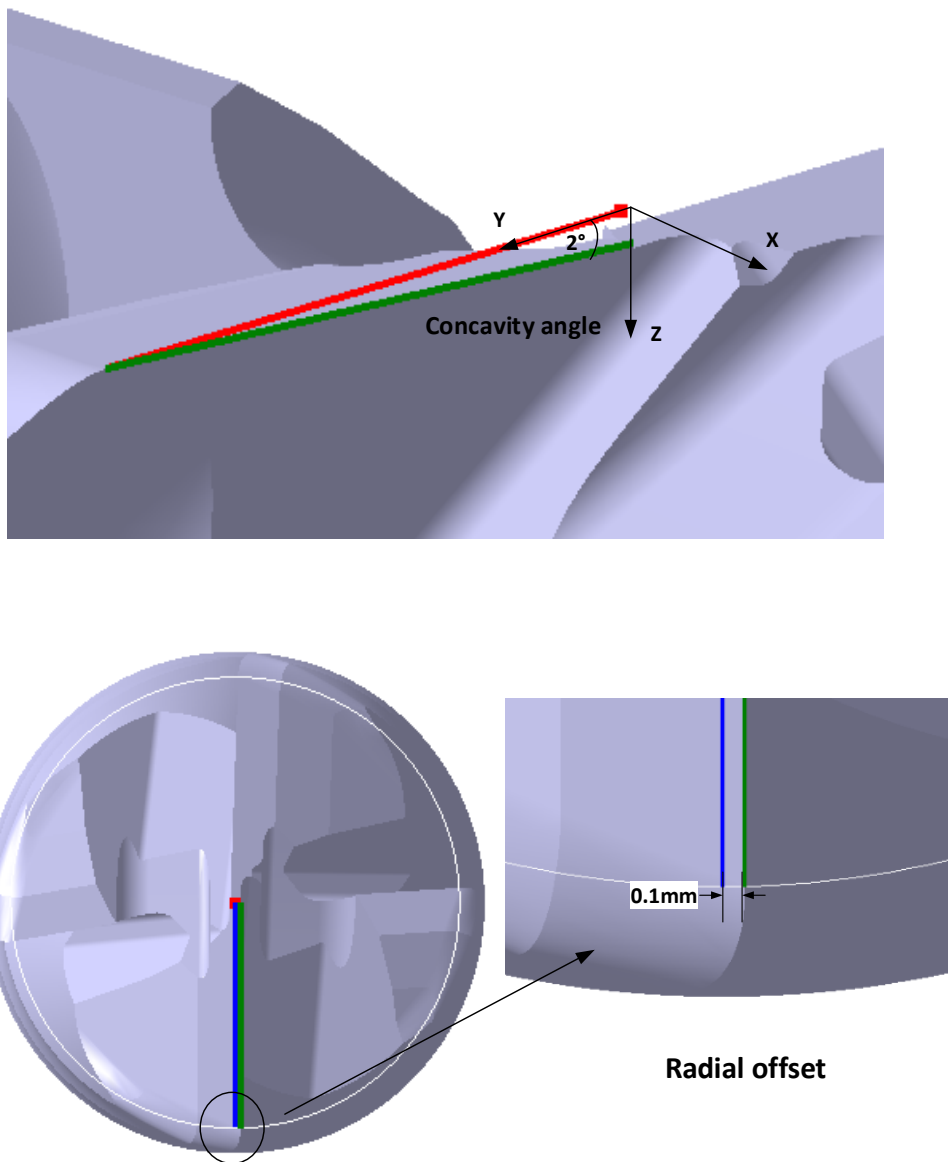


**Figure 2.8 Bottom edge structure**

Since the Equation of early form of bottom cutting edge is derived, mapping method is used to find the Equation of bottom cutting edge:

$$P_{bottomedge} = M_1 M_2 M_3 M_4 M_5 P_{edge} \quad \text{Eq2.3}$$

$$M_1 = \begin{bmatrix} 1 & 0 & 0 & 0 \\ 0 & 1 & 0 & -\left(\frac{D}{2} - R_c\right) \\ 0 & 0 & 1 & 0 \\ 0 & 0 & 0 & 1 \end{bmatrix}$$

$$M_2 = \begin{bmatrix} 1 & 0 & 0 & 0 \\ 0 & \cos(-\alpha_l) & \sin(-\alpha_l) & 0 \\ 0 & -\sin(-\alpha_l) & \cos(-\alpha_l) & 0 \\ 0 & 0 & 0 & 1 \end{bmatrix}$$

$$M_3 = \begin{bmatrix} \cos \theta & \sin \theta & 0 & 0 \\ -\sin \theta & \cos \theta & 0 & 0 \\ 0 & 0 & 1 & 0 \\ 0 & 0 & 0 & 1 \end{bmatrix}$$

$$M_4 = \begin{bmatrix} 1 & 0 & 0 & 0 \\ 0 & 1 & 0 & \frac{D}{2} - R_c \\ 0 & 0 & 1 & 0 \\ 0 & 0 & 0 & 1 \end{bmatrix}$$

$$M_5 = \begin{bmatrix} \cos(-\theta) & \sin(-\theta) & 0 & 0 \\ -\sin(-\theta) & \cos(-\theta) & 0 & 0 \\ 0 & 0 & 1 & 0 \\ 0 & 0 & 0 & 1 \end{bmatrix}$$

where, D is the diameter of the bar,  $R_c$  is the corner radius,  $\alpha_l$  is the concavity angle, the definition of  $\theta$  is shown in Figure 2.9 and calculated via Eq2.4

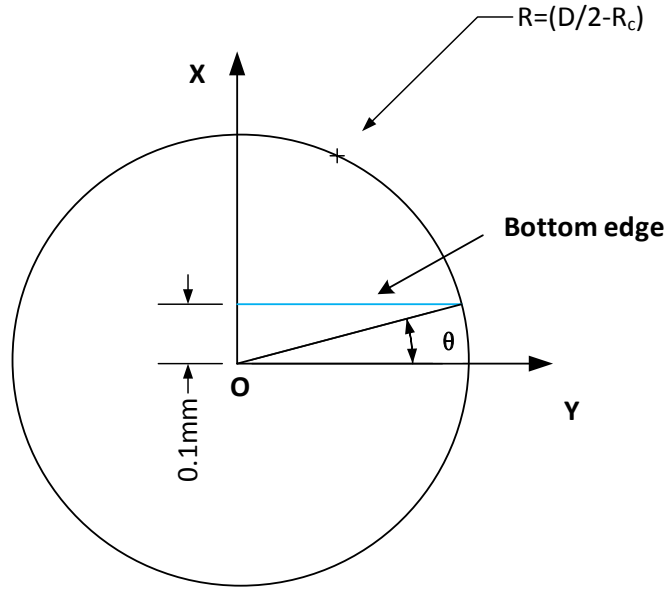


Figure 2.9 The definition of  $\theta$

$$\theta = \sin^{-1} \left( \frac{D_{radialoffset}}{\frac{D}{2} - R_c} \right) \quad \text{Eq2.4}$$

So the parametric Equation of bottom cutting edge is:

$$P_{bottomedge} = \begin{bmatrix} \sin \theta \cdot \left( \frac{D}{2} - R_c \right) \\ R_c - \frac{D}{2} + \cos \alpha_I \cdot \left( \cos \theta \cdot \left( \frac{D}{2} - R_c \right) + l \right) \\ \sin \alpha_I \cdot \left( \cos \theta \cdot \left( \frac{D}{2} - R_c \right) + l \right) \end{bmatrix} \quad \text{Eq2.5}$$

As mentioned before, the orthogonal cutting model can be applied here to create the clearance face of the bottom cutting edge. The orthogonal model of the bottom of the end-mill cutter is shown in Figure 2.10

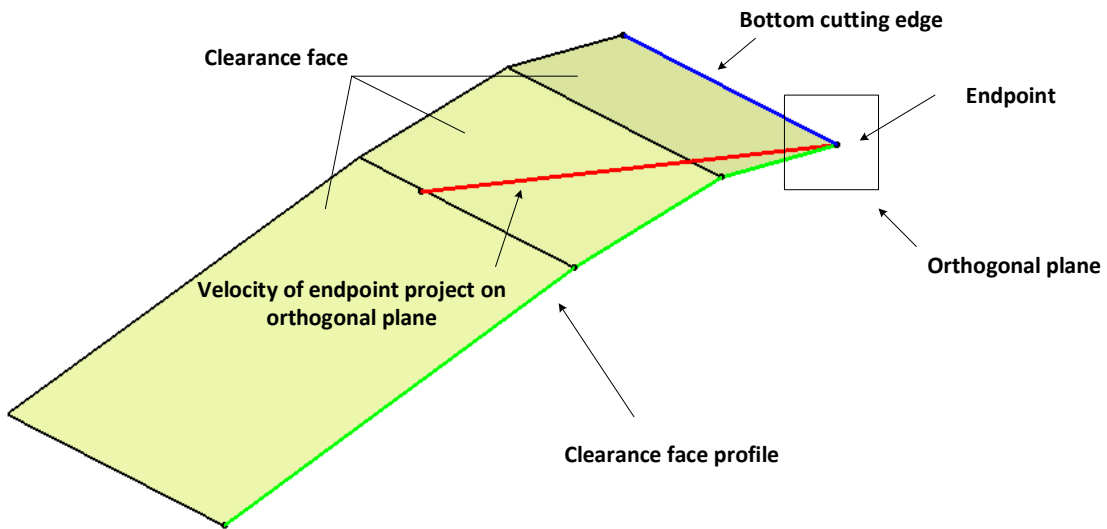


**Figure 2.10 Orthogonal model of bottom clearance face**

The bottom cutting edge and the endpoint can be built using Eq2.5 by substituting parameters in Table2.2. The endpoint is chosen to generate the orthogonal plane which is perpendicular to the bottom cutting edge. Then the clearance profile is defined on the orthogonal plane. With the value of parameters of clearance profile, it can be generated on the orthogonal plane, shown in Figure2.11. The function of sweep surface is used to reach the 3D model of clearance face. By sweeping the bottom cutting edge along clearance profile, the flank faces of bottom edge is derived.

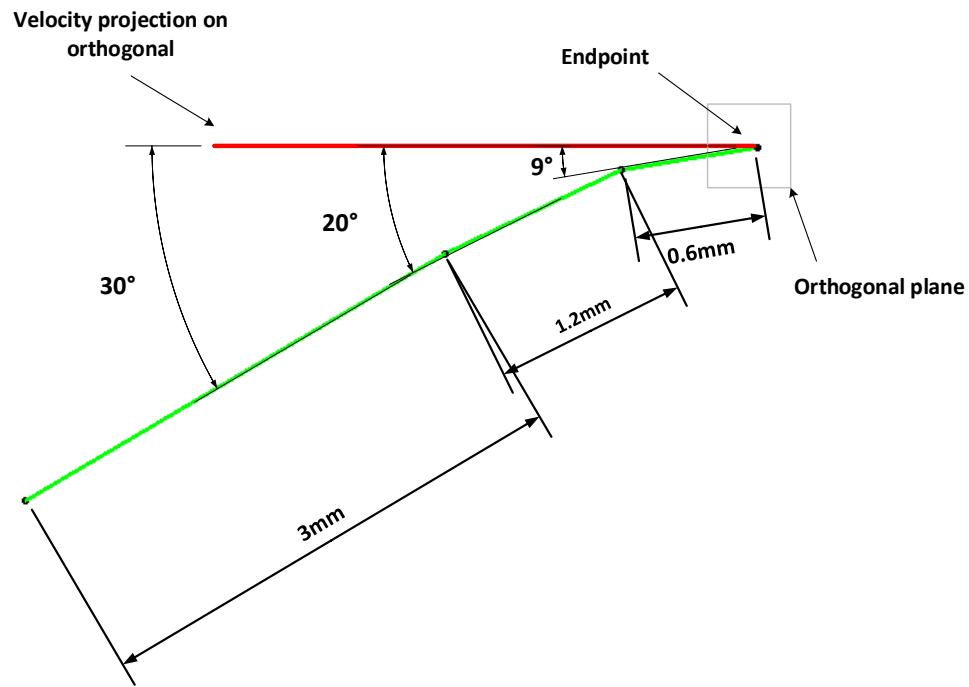


Figure 2.11 Clearance profile

### 2.2.3 Side cutting edge

For flat end-mill cutter, the side edge starts from the intersection of bottom cutting edge and the flute profile, shown in Figure 2.7. The parametric Equation of side cutting edge is:

$$P_{flatsideedge}(d) = \begin{bmatrix} \frac{D}{2} \cdot \cos\left(\frac{2d \cdot \tan \beta}{D} + \frac{\pi}{2}\right) \\ \frac{D}{2} \cdot \sin\left(\frac{2d \cdot \tan \beta}{D} + \frac{\pi}{2}\right) \\ d \end{bmatrix} \quad \text{Eq2.6}$$

$$d \in [0, L_{flute}]$$

Where,  $D$  is the diameter of the bar,  $\beta$  is the helix angle of side edge and  $L_{\text{flute}}$  is the length of flute.

However, for fillet end-mill cutter, the start point of side edge is also the endpoint of the fillet, as shown in Figure 2.12.

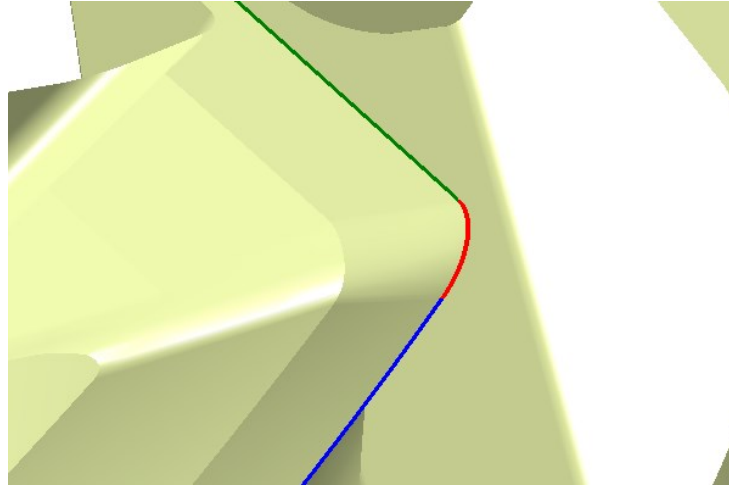


**Figure 2.12 Connection of fillet and side edge**

With the exterior endpoint of flute profile, the start point of side edge is derived by substituting the coordinate of the endpoint of flute profile into a changed form of Eq2.6. Because the exterior endpoint of flute profile is not on one of the axes, for a random point  $P_r(a,b,0)$  on circle, the Equation of helix based on this point is:

$$P_{helixr}(d) = \begin{bmatrix} \frac{D}{2} \cdot \cos\left(\frac{2d \cdot \tan \beta}{D} + \frac{\pi}{2} - \tan^{-1} \frac{a}{b}\right) \\ \frac{D}{2} \cdot \sin\left(\frac{2d \cdot \tan \beta}{D} + \frac{\pi}{2} - \tan^{-1} \frac{a}{b}\right) \\ d \end{bmatrix} \quad \text{Eq2.7}$$

Since the starting point of the side edge is also the endpoint of the 1/4 arc, the  $z$  coordinate of the start point is reached, shown in Figure2.13.

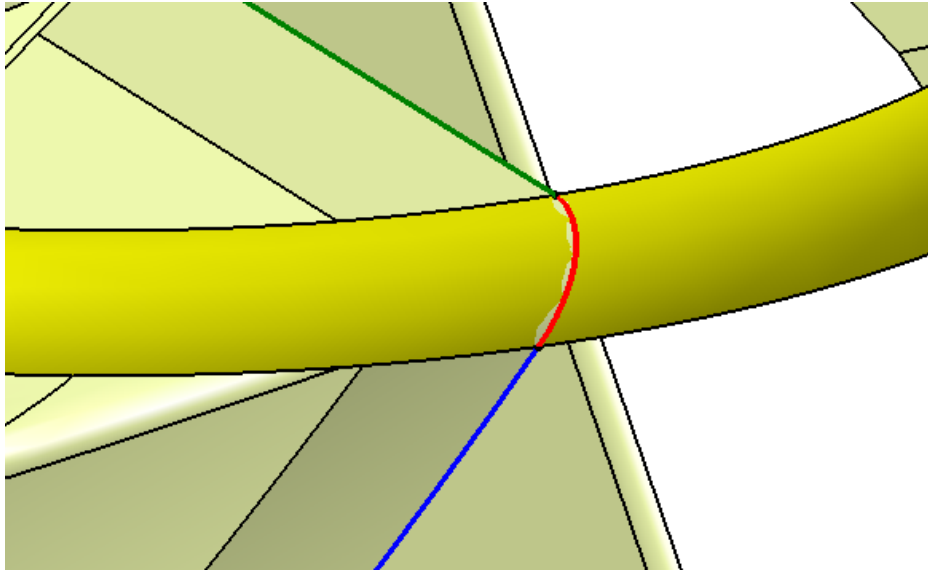


**Figure 2.13 Start point on annular surface**

$$d = R_c$$

By substituting  $d$ ,  $a$  and  $b$  to eq2.7, the coordinate of the starting point of side edge is derived.

Similarly for the side cutting edge, the orthogonal plane is applied to build the clearance faces of side cutting edge. Table2.3 shows the design parameters of side cutting edge. The data of the helix cutting edge has been derived and is used to build it in CAD software. The velocity of the start point is normal to the direction of the radius between the axis of the cutter and this point. The orthogonal plane of side edge is perpendicular to the axis of the cutter and through the start point of side edge. With the orthogonal plane, the side edge profile can be defined. Since the side cutting edge is a helix that around the axis of cutter with constant pitch angle, the clearance face of the side edge can be generated by sweeping the clearance profile along pulling direction, axis of the cutter, with the helix side edge as guide curve, shown in Figure 2.14.

**Table2.3 Design parameters of side cutting edge**

Parameter	definition	value
-----------	------------	-------

$A_{SIDERELIEF1}$	The relief angle of first side flank	9°
$A_{SIDERELIEF2}$	The relief angle of second side flank	25°
$A_{SIDERELIEF3}$	The relief angle of third side flank	30°
$W_{SIDERELIEF1}$	Clearance width of the first side flank	0.6mm
$W_{SIDERELIEF2}$	Clearance width of the second side flank	1.2mm
$W_{SIDERELIEF3}$	Clearance width of the third side flank	3mm

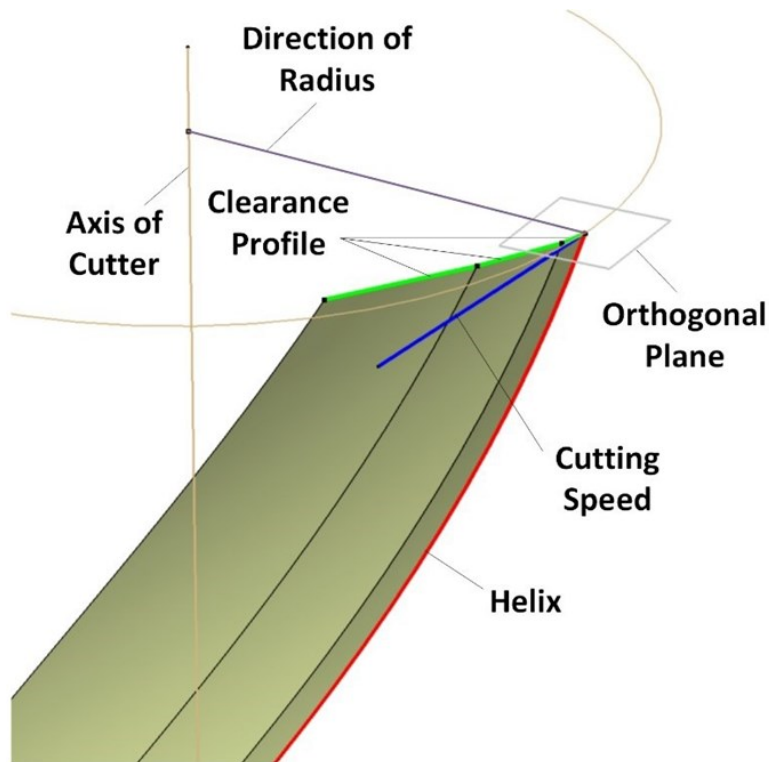
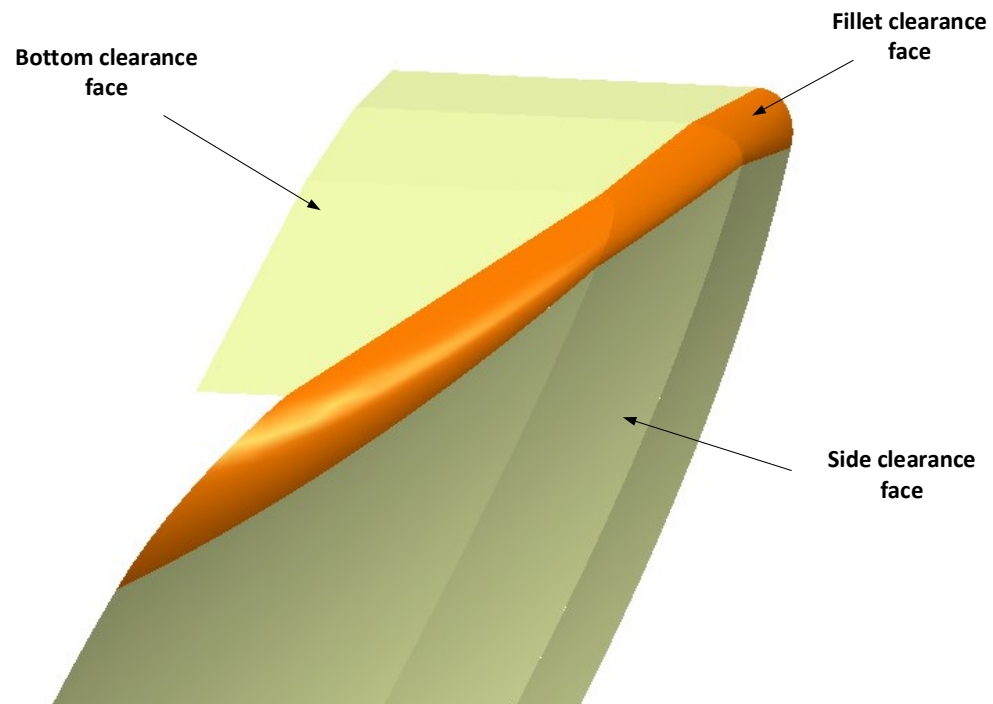


Figure 2.14 Side edge clearance face

#### 2.2.4 Fillet

Fillet is a unique feature that only exists on a fillet end-mill cutter. Geometrically, fillet flank is the connection of bottom flank and side flank, shown in Figure 2.15. The fillet also bring some

advantages for end-mill cutter. Comparing to the other two common end-mill cutters, fillet end-mill cutter has a good strength of the cutting edge which also can machine some work pieces with special requirement, such as leaving a corner on the work piece. However, currently in industry, the machining of fillet is a secret to the designer because the design of fillet is not supplied by the commercial CAM software. Therefore, there is no design parameter available for this feature.



**Figure 2.15 Fillet flank**

In this thesis, a simple function of CATIA, fill surface, is used to create a smooth fillet clearance face and the fillet edge is guaranteed. Fill surface is a function that using several curves as the boundary to build the surface, as shown in Figure 2.16. The flank surface can be generated when the boundary is found.

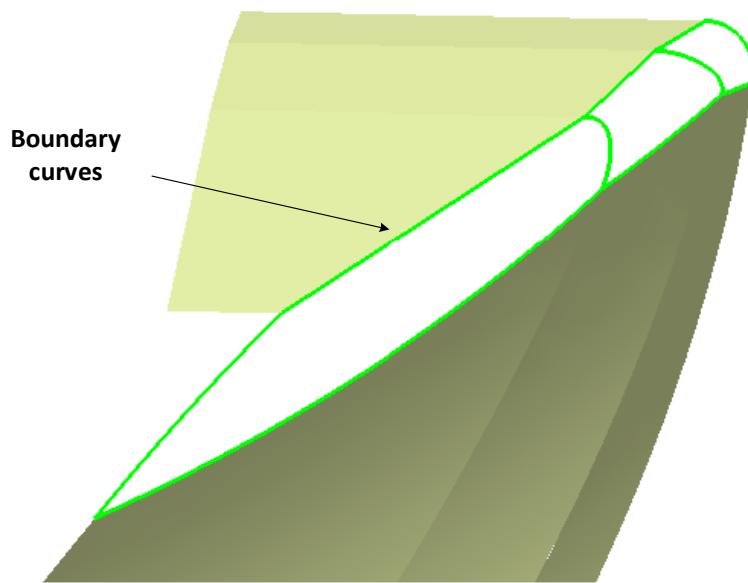


**Figure 2.16 Boundary curves**

Since the end relief surface and the side relief surface are generated by using sweep function, there would be intersection between them. Thus, both of the relief surfaces should be trimmed and replaced by fillet flank surfaces, shown in Figure 2.17.

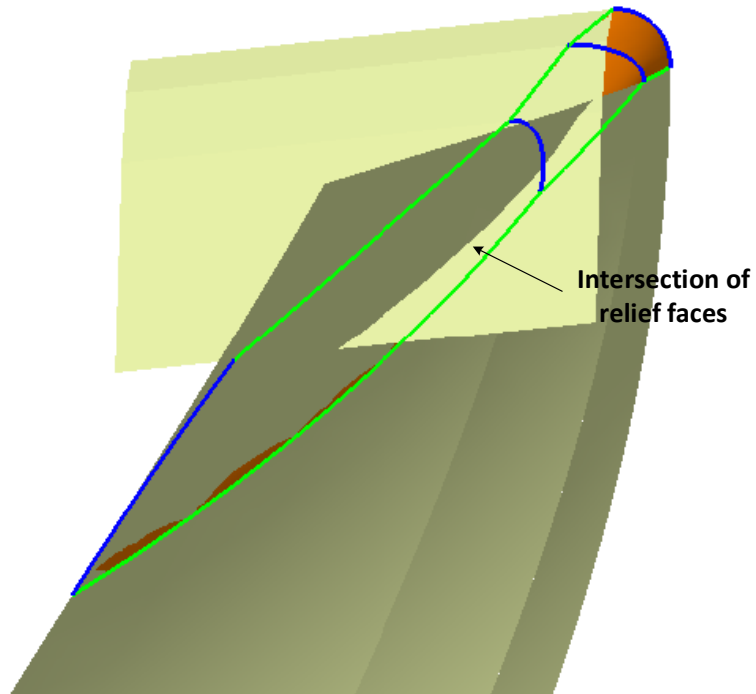


**Figure 2.17 Intersection between bottom and side flank**

The trimmed flank of bottom and side are shown in Figure 2.16. The green boundary line is derived after trimming the intersection part. For the four blue boundary lines, different functions are applied.

Fillet edge is formed by the flute profile that sweep along the helix line. To build it, the Equation is derived. For the helix line that start from different points on flute profile, parametric

Equation is:

$$P_{flutehelix}(d) = \begin{bmatrix} \sqrt{a^2 + b^2} \cdot \cos\left(\tan^{-1} \frac{a}{b} + \frac{d \cdot \tan \beta}{\sqrt{a^2 + b^2}}\right) \\ \sqrt{a^2 + b^2} \cdot \sin\left(\tan^{-1} \frac{a}{b} + \frac{d \cdot \tan \beta}{\sqrt{a^2 + b^2}}\right) \\ d \end{bmatrix} \quad \text{Eq2.8}$$

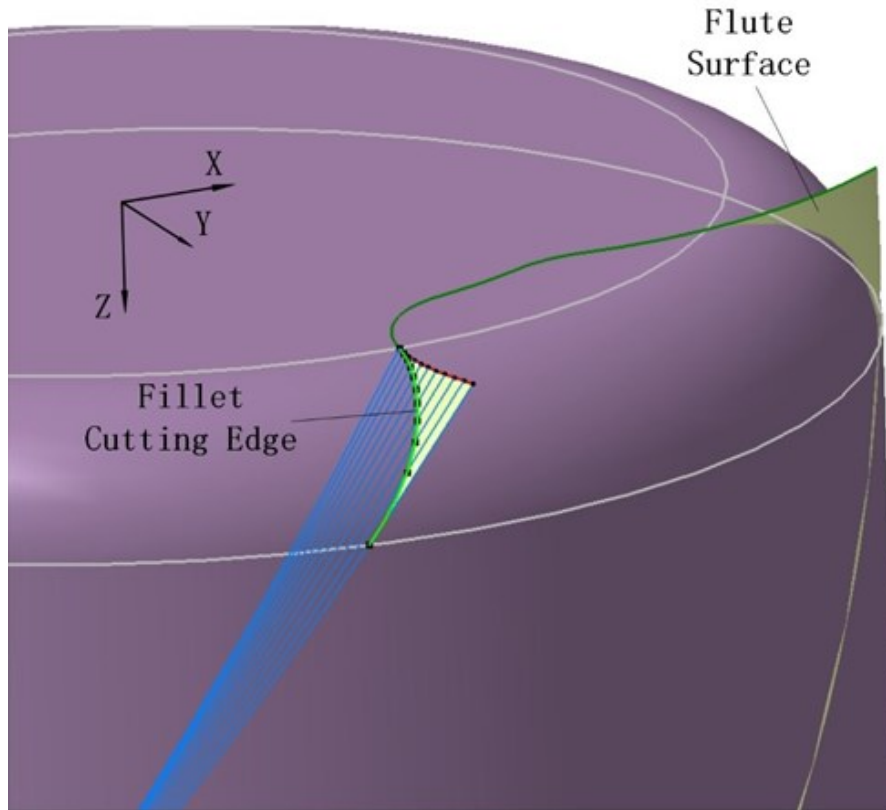


**Figure 2.18 Fillet cutting edge**

The intersection points between flute surface and helix line consist of fillet cutting edge. Thus, the points are derived:

$$\begin{cases} \left(\frac{D}{2} - R_c + R_c * \cos \delta\right) * \cos \mu = \sqrt{a^2 + b^2} \cdot \cos\left(\tan^{-1} \frac{a}{b} + \frac{d \cdot \tan \beta}{\sqrt{a^2 + b^2}}\right) \\ \left(\frac{D}{2} - R_c + R_c * \cos \delta\right) * \sin \mu = \sqrt{a^2 + b^2} \cdot \sin\left(\tan^{-1} \frac{a}{b} + \frac{d \cdot \tan \beta}{\sqrt{a^2 + b^2}}\right) \\ R_c - R_c * \sin \delta = d \end{cases} \quad \text{Eq2.9}$$

By solving the Equation set, the fillet cutting edge is reached and can be built. There is no rule for the other three blue boundary lines so the connecting curve function is applied. With this function, a connect line, where the endpoints are on the two side edges, between two side edges is created under given rules, shown in Figure 2.19.

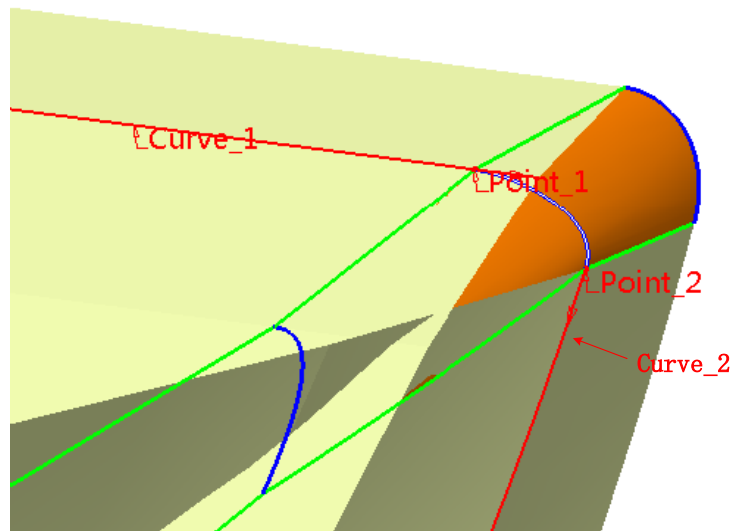


**Figure 2.19 Connect curve**

Since all the boundaries are found, fill surface function is used, as shown in Figure 2.21.

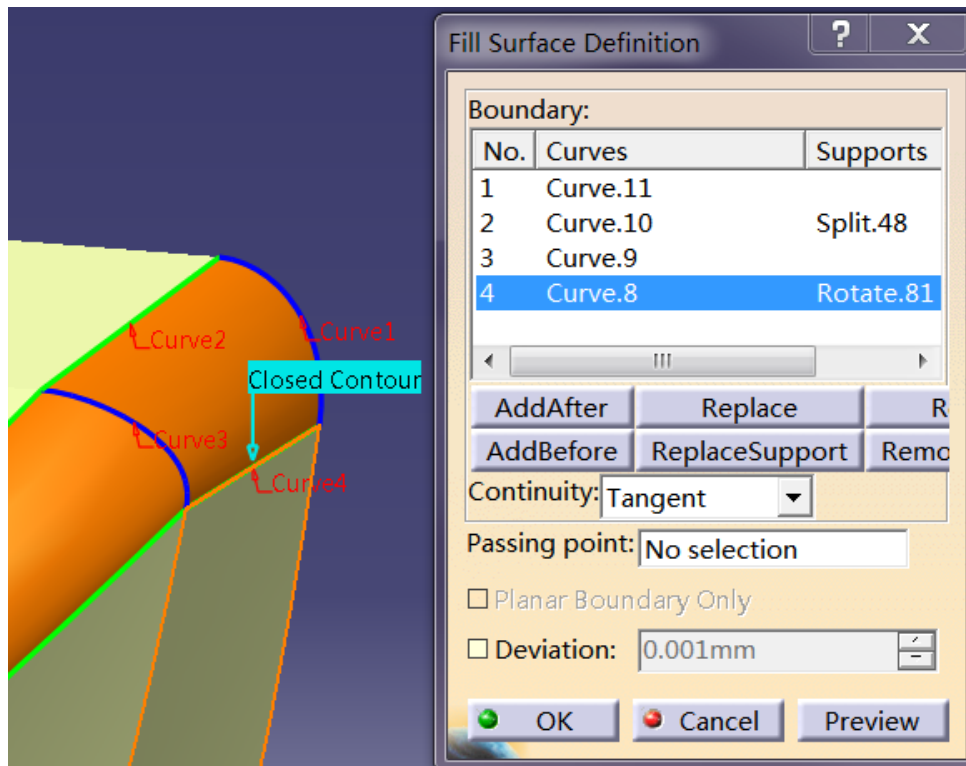


**Figure 2.20 Fill surface function**

# CHAPTER 3 FEATURE MODELING OF GASH

## 3.1 Introduction

Gash is a significant feature for a cutting tool. The function of gash is similar as the flute to side edge. Gash is a space that includes the rake face of bottom cutting edge. During milling process, gash is used to evacuate and break chips, shown in Figure 3.1.

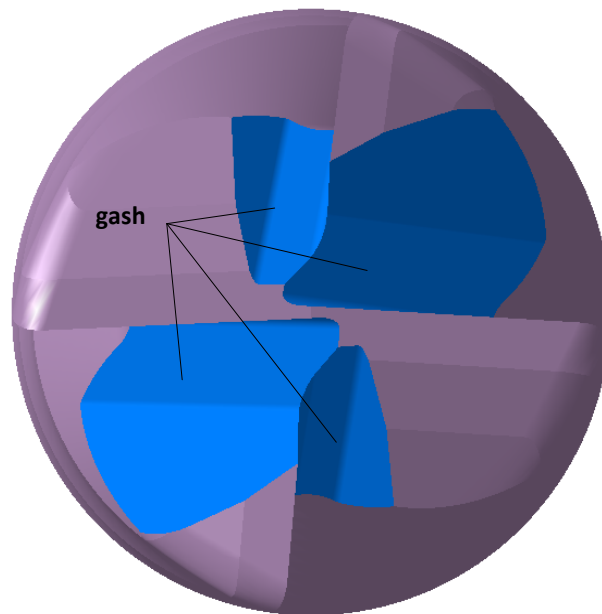


**Figure 3.1 Gash**

Therefore, the design of gash could have great influences on the cutting tool performance. If the gash is too small, as shown in Figure 3.2, chips could not be evacuated smoothly. Then chips may stack there and affect the finish surface. During cutting process, friction force between chips

and rake face will generate heat. With less space of gash, the heat transmission rate of bottom cutting edge area is low. Thus, the temperature of this area will increase and high temperature will soften the cutting tool. Finally, failure occurs at the cutting process. On the other hand, if the space of gash is large, the strength of the bottom cutting edge will decrease, shown in Figure 3.2.

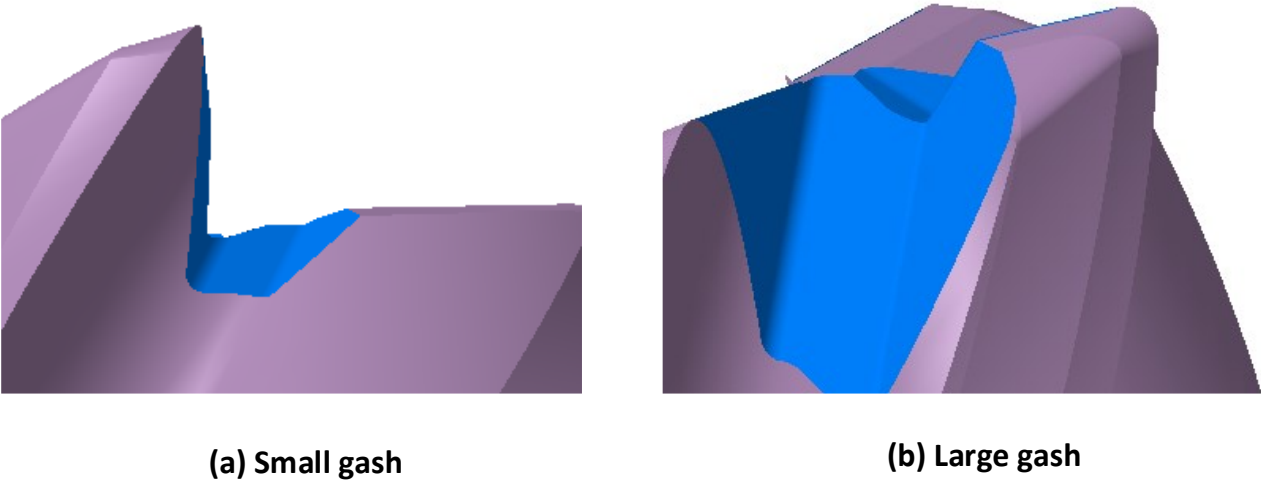


Figure 3.2 Gash comparison

As mentioned before, gash is also machined by grinding wheel. First, the grinding wheel will approach to the end-mill cutter to make the rake face of bottom edge. Then, the grinding wheel will move away from the rake face along the direction that is perpendicular to the rake face, as shown in Figure 3.3.

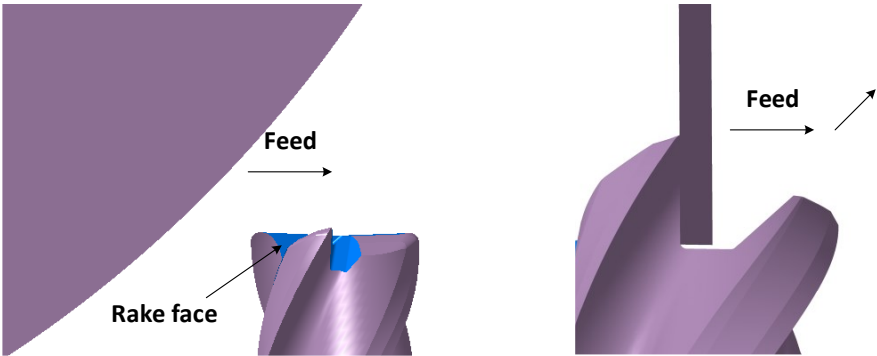


Figure 3.3 Gash machining process

The design parameters of gash are listed in Table 3.1.

**Table 3.1 Design parameters of gash1**

Parameters	Definition	Value
$W_{depth1}$	Distance between the deepest point machined by grinding wheel and the vertical plane pass through bottom cutting edge	0.4mm
$W_{width1}$	Width of the gash	1.4mm
$R_{gashcorner1}$	Corner radius of gash profile	0.2mm
$\alpha_{guide1}$	Angle between guide line of gash profile and XY plane	40°
$\alpha_{gash1open}$	Gash profile open angle	55°
$\alpha_{gash1bottm}$	Angle between bottom line and side line of gash profile	90°

Data of Table 3.1 expresses two aspects information about gash. First, the shape of gash profile is formed with the constraints above. Then the location of gash is ensured with respect to the limitations above.

The constraints of gash location are stated clearly, as shown in Figure 3.4. The red line is the bottom cutting edge. The green line is the intersection of first clearance face and second clearance face. The black point is the intersection of gash and green line. The yellow point is the deepest position that gash left on the first flank. The plane is perpendicular to the red bottom cutting edge and through origin point. By controlling the distance between black point and the white plane, gash width is derived. Also the distance of yellow point and the black plane is used to reach the cutting depth. The guide direction is a line that belongs to rake plane and has an angle of 40° with

respect to XY plane.

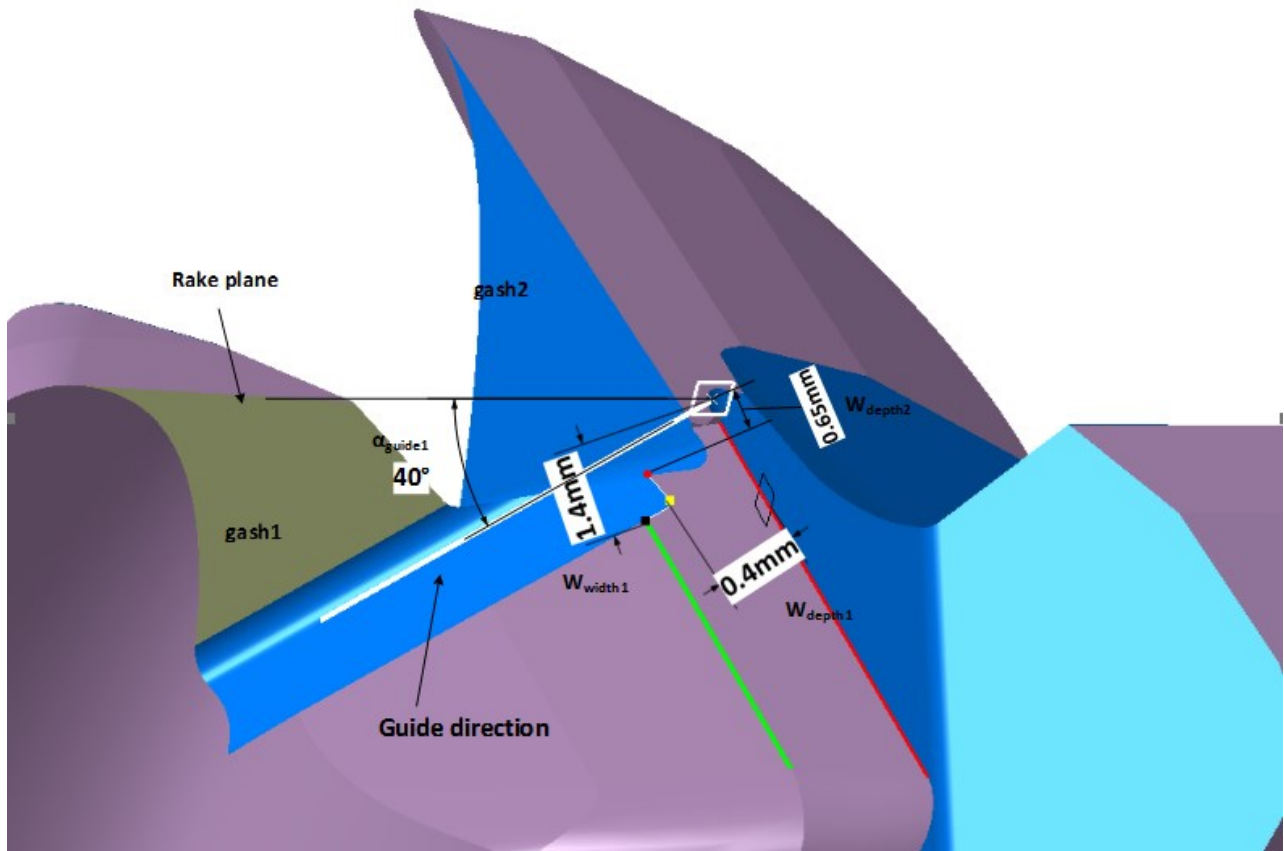
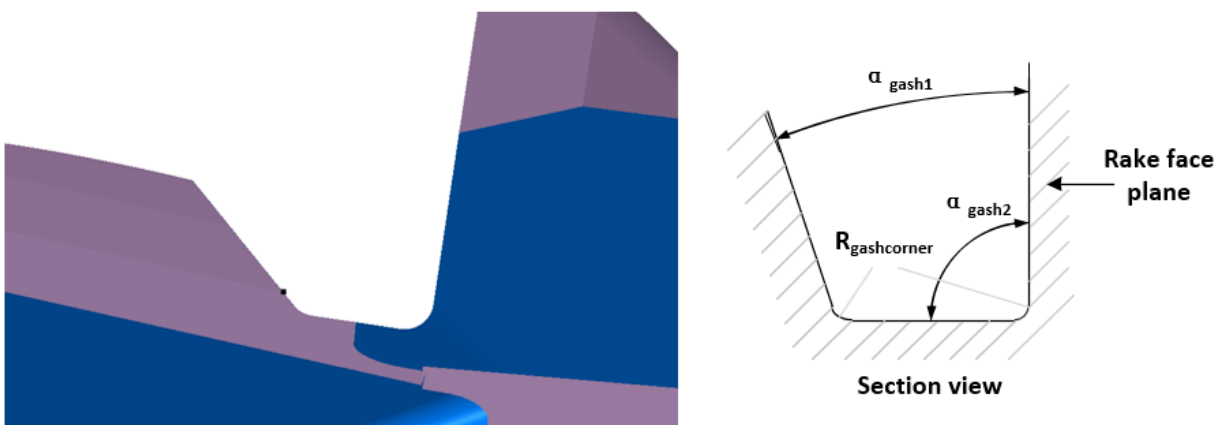


Figure 3.4 Parameter illustration

As mentioned before, the constraints of gash reflect two parts, besides gash position, restrictions of gash profile are shown in Figure 3.5



**Figure 3.5 Gash profile**

With the sweep surface function in CATIA, the gash can be built using gash profile that sweeps along guide direction. As the gash is machined by a grinding wheel, the real shape of gash is not similar to the one that is described before, which consists of three planes. However, the radius of grinding wheel is too large while comparing to the radius of cutting tool bar. So the gash that generated in CAD software is really close to the real shape of gash on the cutter, as shown in Figure 3.6.



**Figure 3.6 Gash comparison**

As referred in Chapter2, the area of rake face that closes to cutting edge can affects the cutting process. By comparing the two shapes above, it is obvious that the working parts of rake

face are the same, and the shapes are almost the same. Therefore, the model can be used in simulation software and will reflect real cutting dynamics.

### 3.2 Guide direction

To derive the gash in CATIA, the modeling method is discussed before. The sweep surface function is applied to build the gash surface. There are two factors about sweep surface function. In this section, the guide direction is discussed and found. The guide direction is a line that has an angle  $40^\circ$  with respect to XY plane, this guide line is also belong to the rake face plane, as shown in Figure 3.7.

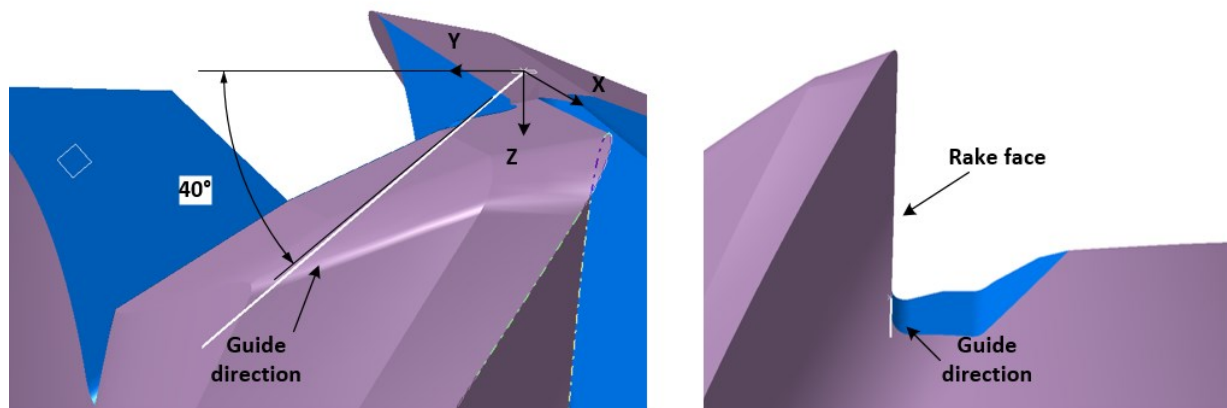


**Figure 3.7 Guide direction**

Since the rake face does not coincide with one of the given plane and the guide direction belongs to this plane, the rake face should be found first. As shown in Figure 2.3, the rake face has an angle of  $\alpha$ , which is the rake angle, with respect to the vertical plane. The vertical plane is a plane that goes through cutting edge and is normal to the direction of velocity. The cutting edge

belongs to rake face as well. So the rake face can be derived by rotating the vertical plane around velocity direction by  $\alpha$  degree. The vertical plane is defined and shown in Figure 3.8.

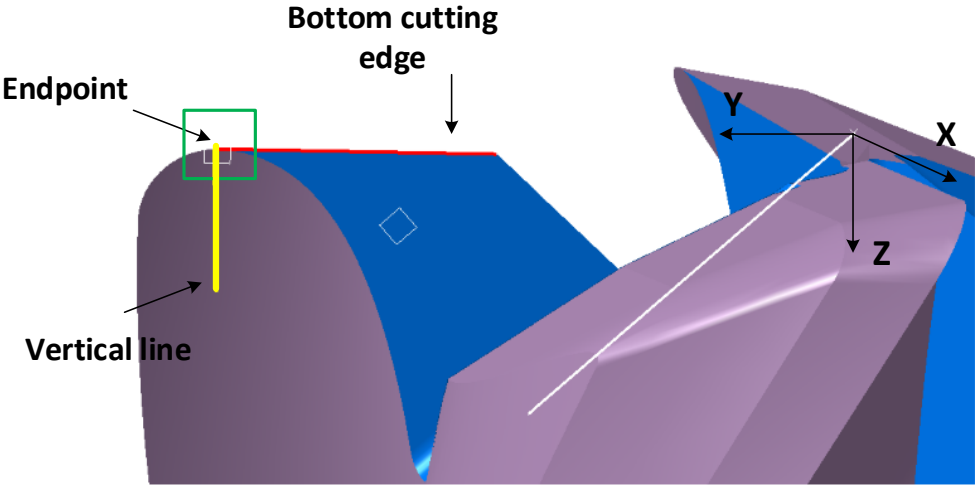


**Figure 3.8 Vertical plane**

The red line is the bottom cutting edge. The yellow line is a vertical line which is parallel to Z-axis, meanwhile the intersection of vertical line and red line is the endpoint of bottom cutting edge. The green plane is the target plane which is perpendicular to the velocity and pass through the bottom cutting edge. Then rotating the green plane around bottom cutting edge by  $\alpha$ , the rake face plane is found, as shown in Figure 3.9.

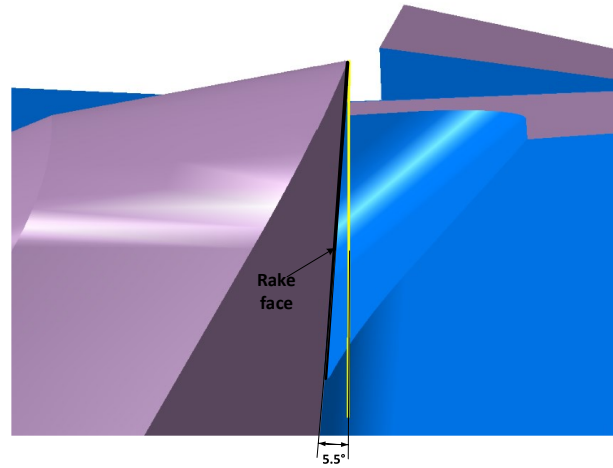


**Figure 3.9 Rake face**

A norm vector of the rake face is used to represent the Equation of this rake face. From Figure 3.8 and Figure 3.9, the rake face is derived by rotating the green plane around the red cutting edge by  $\alpha$ . Similarly for the norm vector, the norm vector of rake face can be developed by rotating the norm vector of green plane around cutting edge by  $\alpha$  and it is easy to find the norm vector of green plane. The norm vector of rake face is:

$$\vec{n}_{rake} = M_5 M_4 M_3 M_2 M_1 \vec{n}_{vertical} \quad \text{Eq3.1}$$

$$\vec{n}_{vertical} = \begin{bmatrix} 1 \\ 0 \\ 0 \end{bmatrix}$$

$$M_1 = \begin{bmatrix} 1 & 0 & 0 & 0 \\ 0 & 1 & 0 & -y_1 \\ 0 & 0 & 1 & 0 \\ 0 & 0 & 0 & 1 \end{bmatrix}$$

$$M_2 = \begin{bmatrix} 1 & 0 & 0 & 0 \\ 0 & \cos \alpha_I & \sin \alpha_I & 0 \\ 0 & -\sin \alpha_I & \cos \alpha_I & 0 \\ 0 & 0 & 0 & 1 \end{bmatrix}$$

$$M_3 = \begin{bmatrix} \cos(-\alpha_{rake}) & 0 & -\sin(-\alpha_{rake}) & 0 \\ 0 & 1 & 0 & 0 \\ \sin(-\alpha_{rake}) & 0 & \cos(-\alpha_{rake}) & 0 \\ 0 & 0 & 0 & 1 \end{bmatrix}$$

$$M_4 = \begin{bmatrix} 1 & 0 & 0 & 0 \\ 0 & \cos(-\alpha_I) & \sin(-\alpha_I) & 0 \\ 0 & -\sin(-\alpha_I) & \cos(-\alpha_I) & 0 \\ 0 & 0 & 0 & 1 \end{bmatrix}$$

$$M_5 = \begin{bmatrix} 1 & 0 & 0 & 0 \\ 0 & 1 & 0 & y_1 \\ 0 & 0 & 1 & 0 \\ 0 & 0 & 0 & 1 \end{bmatrix}$$

where  $\alpha_I$  is the concavity angle of the cutting edge,  $\alpha_{rake}$  is the rake angle of the cutting edge and the coordinate of endpoint is:

$$P_{endpoint} = \begin{bmatrix} 0 \\ y_1 \\ 0 \end{bmatrix}$$

So the norm vector of rake face is:

$$\vec{n}_{rake} = \begin{bmatrix} \cos \alpha_{rake} + y_1 \cdot \sin \alpha_I \cdot \sin \alpha_{rake} \\ y_1 + \sin \alpha_I \cdot \sin \alpha_{rake} - y_1 \cdot (\cos^2 \alpha_I + \cos \alpha_{rake} \cdot \sin^2 \alpha_I) \\ -y_1 \cdot (\cos \alpha_I \cdot \sin \alpha_I \cdot (1 - \cos \alpha_{rake})) - \cos \alpha_I \cdot \sin \alpha_{rake} \end{bmatrix} \quad \text{Eq3.2}$$

And the rake plane also pass through the end point, as shown in Figure 3.9. So the Equation of rake plane is expressed as:

$$n_{x1} \cdot x + n_{y1} \cdot (y - y_1) + n_{z1} \cdot z = 0 \quad \text{Eq3.3}$$

where

$$\vec{n}_{rake} = \begin{bmatrix} n_{x1} \\ n_{y1} \\ n_{z1} \end{bmatrix}$$

As mentioned above, the guide direction line is on rake face plane, the angle between guide line and XY plane is 40°. Cone is introduced to find the guide line. A right triangle rotates around one of its right-angle sides can leads to a cone. The conical surface is generated by the hypotenuse rotate around right-angle side. If a plane that is parallel to the base of the cone and goes through the vertex of the cone, then the angle between each generatrix of the cone and the parallel plane is Equal, as shown in Figure 3.10.

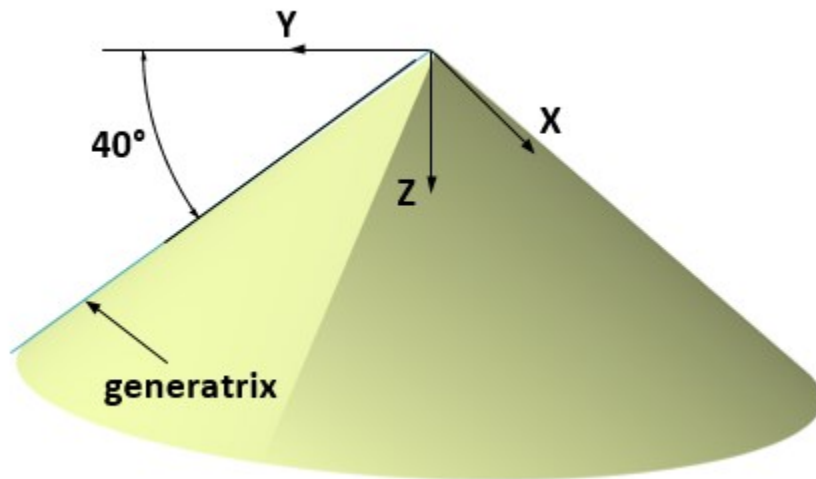


**Figure 3.10 Cone property**

With this property, a conical surface is built by a line, on YZ plane and start from origin, which rotates around Z-axis. Also this generatrix line has an angle of 40° with respect to Y-axis. Then the intersection of conical surface and rake face is the rEqired guide direction, as shown in Figure 3.11. The method can be applied to generate guide direction of both gash1 and gash2.

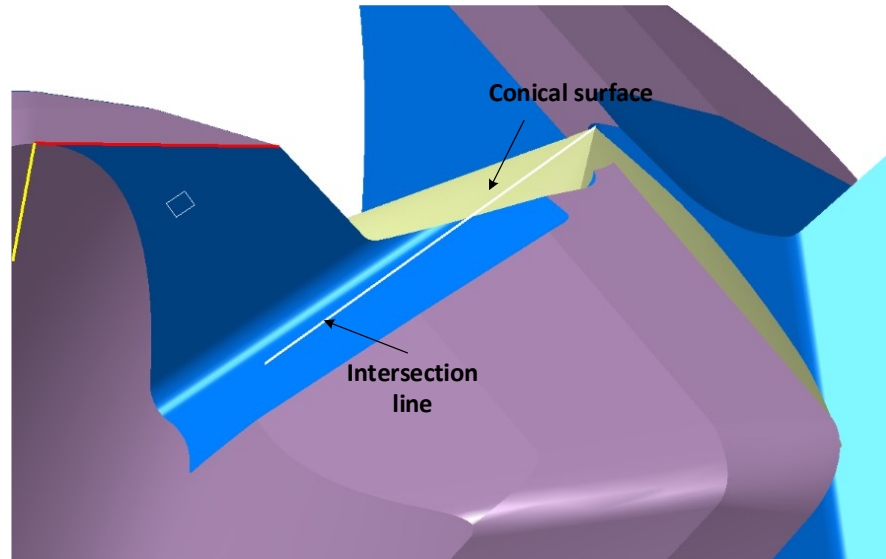


**Figure 3.11 Guide line**

The parametric Equation of conic surface in Figure 3.10 is:

$$S_{cone}(t, \theta) = \begin{bmatrix} t \cdot \tan 50^\circ \cdot \cos \theta \\ t \cdot \tan 50^\circ \cdot \sin \theta \\ t \end{bmatrix} \quad \text{Eq3.4}$$

Assume  $P_{guide}(x_g, y_g, 1)$  is a point on the guide line, so the coordinate of the point can be obtained by solving the Equations below:

$$\begin{cases} n_{x1} \cdot x_g + n_{y1} \cdot (y_g - y_1) + n_{z1} = 0 \\ \tan 50^\circ \cdot \cos \theta = x_g \\ \tan 50^\circ \cdot \sin \theta = y_g \end{cases} \quad \text{Eq3.5}$$

So the parametric Equation of guide line is:

$$P_{guide}(t) = \begin{bmatrix} x_g + x_g \cdot t \\ y_g + y_g \cdot t \\ 1 + t \end{bmatrix} \quad \text{Eq3.6}$$

### 3.3 Gash profile

Since the guide direction line is found, the gash can be formed after the gash profile is derived. As shown in Figure 3.5, data has been collected from section view. So the first step is to find a plane to build gash profile. From Figure 3.4, the black point is selected to be the basic element of this plane. Geometrically, this plane is normal to guide direction line and pass through the black point. The coordinate of black point should be found first to reach the Equation of base plane. Assume the cutting edge coincides with y-axis, and the coordinate of black point is calculated and shown in Figure 3.12.

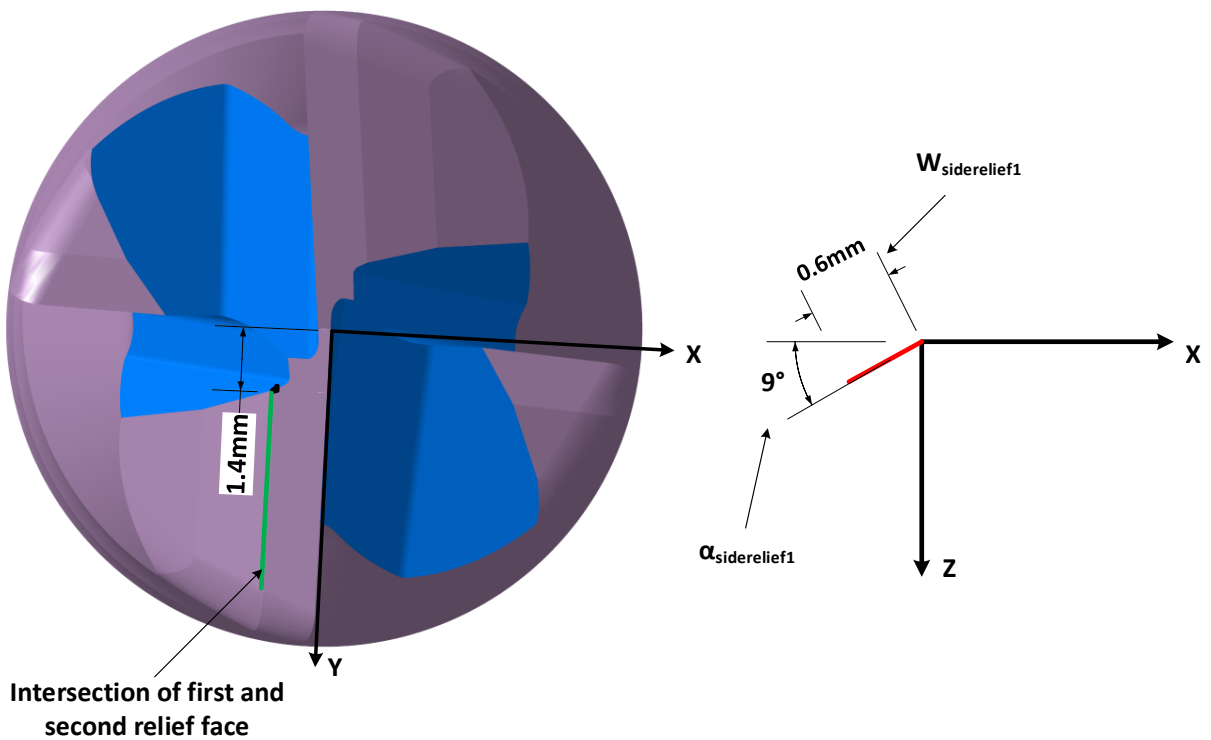


**Figure 3.12 Coordinate of black point**

With the cutting edge coincide with y-axis, the coordinate of black point is:

$$P'_{black} = \begin{bmatrix} -W_{siderelief1} \cdot \cos \alpha_{siderelief1} \\ W_{width1} \\ W_{siderelief1} \cdot \sin \alpha_{siderelief1} \end{bmatrix} \quad \text{Eq3.7}$$

From eq2.3, the bottom edge is developed by applying mapping method. The same

transformation is applied to get the coordinate of black point:

$$P_{black} = M_1 M_2 M_3 M_4 M_5 P'_{black} \quad \text{Eq3.8}$$

where,

$$M_1 = \begin{bmatrix} 1 & 0 & 0 & 0 \\ 0 & 1 & 0 & -\left(\frac{D}{2} - R_c\right) \\ 0 & 0 & 1 & 0 \\ 0 & 0 & 0 & 1 \end{bmatrix}$$

$$M_2 = \begin{bmatrix} 1 & 0 & 0 & 0 \\ 0 & \cos(-\alpha_l) & \sin(-\alpha_l) & 0 \\ 0 & -\sin(-\alpha_l) & \cos(-\alpha_l) & 0 \\ 0 & 0 & 0 & 1 \end{bmatrix}$$

$$M_3 = \begin{bmatrix} \cos \theta & \sin \theta & 0 & 0 \\ -\sin \theta & \cos \theta & 0 & 0 \\ 0 & 0 & 1 & 0 \\ 0 & 0 & 0 & 1 \end{bmatrix}$$

$$M_4 = \begin{bmatrix} 1 & 0 & 0 & 0 \\ 0 & 1 & 0 & \frac{D}{2} - R_c \\ 0 & 0 & 1 & 0 \\ 0 & 0 & 0 & 1 \end{bmatrix}$$

$$M_5 = \begin{bmatrix} \cos(-\theta) & \sin(-\theta) & 0 & 0 \\ -\sin(-\theta) & \cos(-\theta) & 0 & 0 \\ 0 & 0 & 1 & 0 \\ 0 & 0 & 0 & 1 \end{bmatrix}$$

So the Equation of base plane is expressed as:

$$x_g(x - x_{pb}) + y_g(y - y_{pb}) + (z - z_{pb}) = 0 \quad \text{Eq3.9}$$

Where,

$$P_{black} = \begin{bmatrix} x_{pb} \\ y_{pb} \\ z_{pb} \end{bmatrix}$$

From the section view, the gash profile consists of two side lines, a bottom line and two connect corners. Obviously, the side line that belongs to rake face is the intersection line of rake face and base plane, as shown in Figure 3.12. By solving the Equation group of Eq3.3 and Eq3.9 below, the intersection side line is found:

$$\begin{cases} x_g(x - x_{pb}) + y_g(y - y_{pb}) + (z - z_{pb}) = 0 \\ n_{x1} \cdot x + n_{y1} \cdot (y - y_1) + n_{z1} \cdot z = 0 \end{cases}$$

With  $z=0$ , the coordinate of a point on the intersection side line is defined:

$$P_{intersection} = \begin{bmatrix} x_{intersection} \\ y_{intersection} \\ 0 \end{bmatrix}$$

Then the direction vector of intersection side line is:

$$\vec{d}_{intersection} = \vec{n}_{rake} \times \vec{n}_{base}$$

where  $\vec{n}_{rake}$  is the norm vector of rake face,  $\vec{n}_{base}$  is the norm vector of base plane. So the parametric Equation of intersection side line is:

$$P_{sideline1}(t) = \begin{bmatrix} x_{intersection} + d_{xi1} \cdot t \\ y_{intersection} + d_{yi1} \cdot t \\ d_{zi1} \cdot t \end{bmatrix} \quad \text{Eq3.10}$$

and

$$\vec{d}_{intersection} = \begin{bmatrix} d_{xi1} \\ d_{yi1} \\ d_{zi1} \end{bmatrix}$$

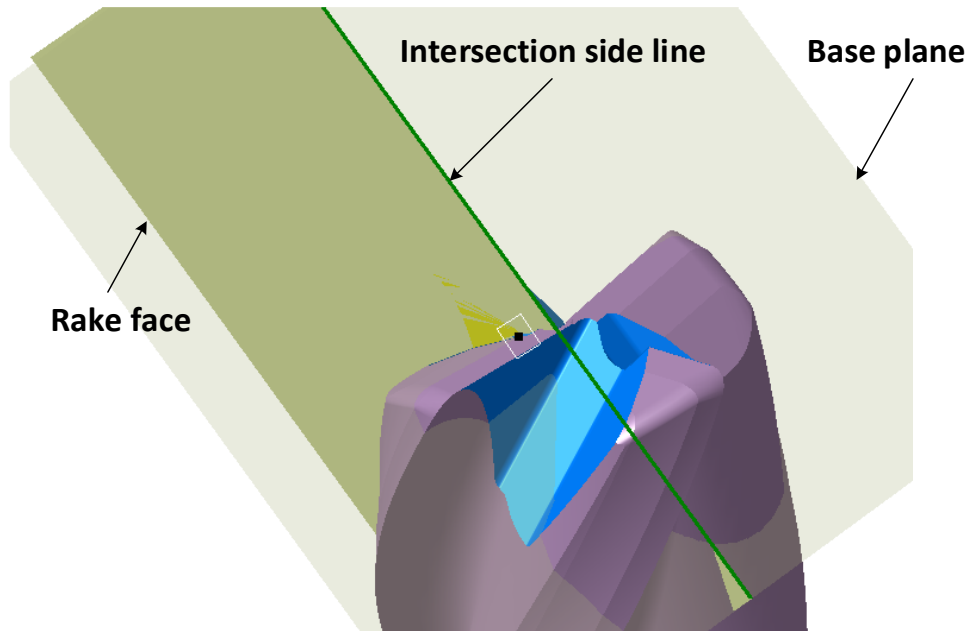


**Figure 3.13 Intersection side line**

The black point referred before is on the other side line of gash profile. Through this black point and on the base plane, the second side line of gash profile is created with an angle of  $55^\circ$  in terms of first side line, as shown in Figure 3.13.

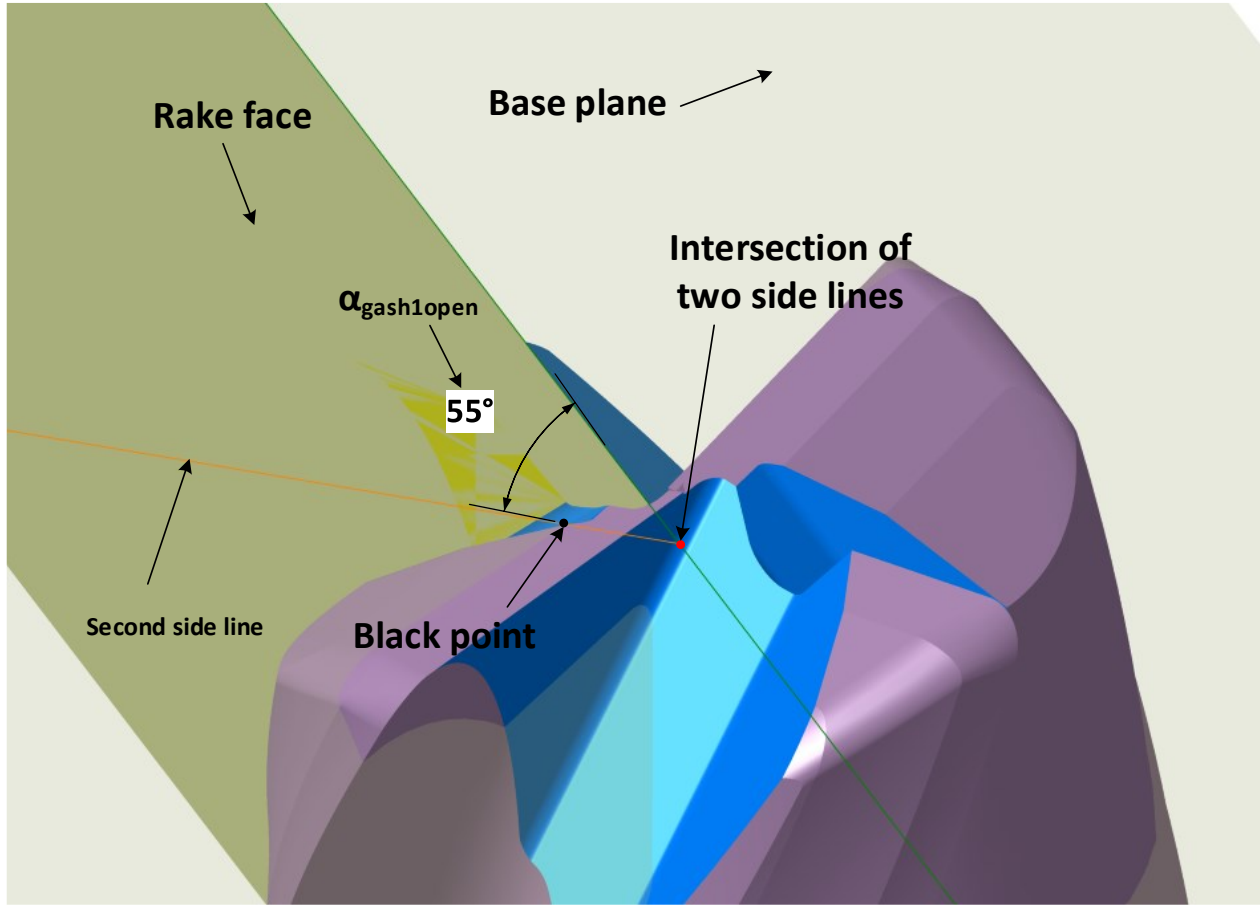


Figure 3.14 Second side line

Supposely, the coordinate of intersection point about two side lines is:

$$P_{ir} = \begin{bmatrix} x_{ir} \\ y_{ir} \\ z_{ir} \end{bmatrix}$$

An Equation group is obtained with the geometrical feature shown in Figure 3.13. Firstly,  $P_{ir}$  is on the rake face; And  $P_{ir}$  is on the base plane as well. Finally, the direction vector of this two side line has an angle of  $55^\circ$ . So the Equation group is:

$$\begin{cases} n_{x1} \cdot x_{ir} + n_{y1} \cdot (y_{ir} - y_1) + n_{z1} \cdot z_{ir} = 0 \\ x_g(x_{ir} - x_{pb}) + y_g(y_{ir} - y_{pb}) + (z_{ir} - z_{pb}) = 0 \\ \frac{d_{xi1}(x_{pb} - x_{ir}) + d_{yi1}(y_{pb} - y_{ir}) + d_{zi1}(z_{pb} - z_{ir})}{\sqrt{d_{xi1}^2 + d_{yi1}^2 + d_{zi1}^2} \cdot \sqrt{(x_{pb} - x_{ir})^2 + (y_{pb} - y_{ir})^2 + (z_{pb} - z_{ir})^2}} = \cos \alpha_{gash1open} \end{cases}$$

By solving the Equation above, the coordinate of the intersection point is achieved. Then, the parametric Equation of orange side line is expressed as:

$$P_{sideline2}(t) = \begin{bmatrix} x_{pb} + (x_{pb} - x_{ir}) \cdot t \\ y_{pb} + (y_{pb} - y_{ir}) \cdot t \\ z_{pb} + (z_{pb} - z_{ir}) \cdot t \end{bmatrix} \quad \text{Eq3.11}$$

The cutting depth  $W_{depth1}$  is used to confine the position of bottom line. Firstly, a vertical plane which includes the long cutting edge is generated. Then, an offset plane which is parallel to vertical plane is built and the distance between two planes is 0.4mm. Besides, the parallel plane intersects with first clearance that leads to the black intersection line. Finally, projecting the intersection line on base plane, the constraint of the bottom line is reached, as shown in Figure 3.13.

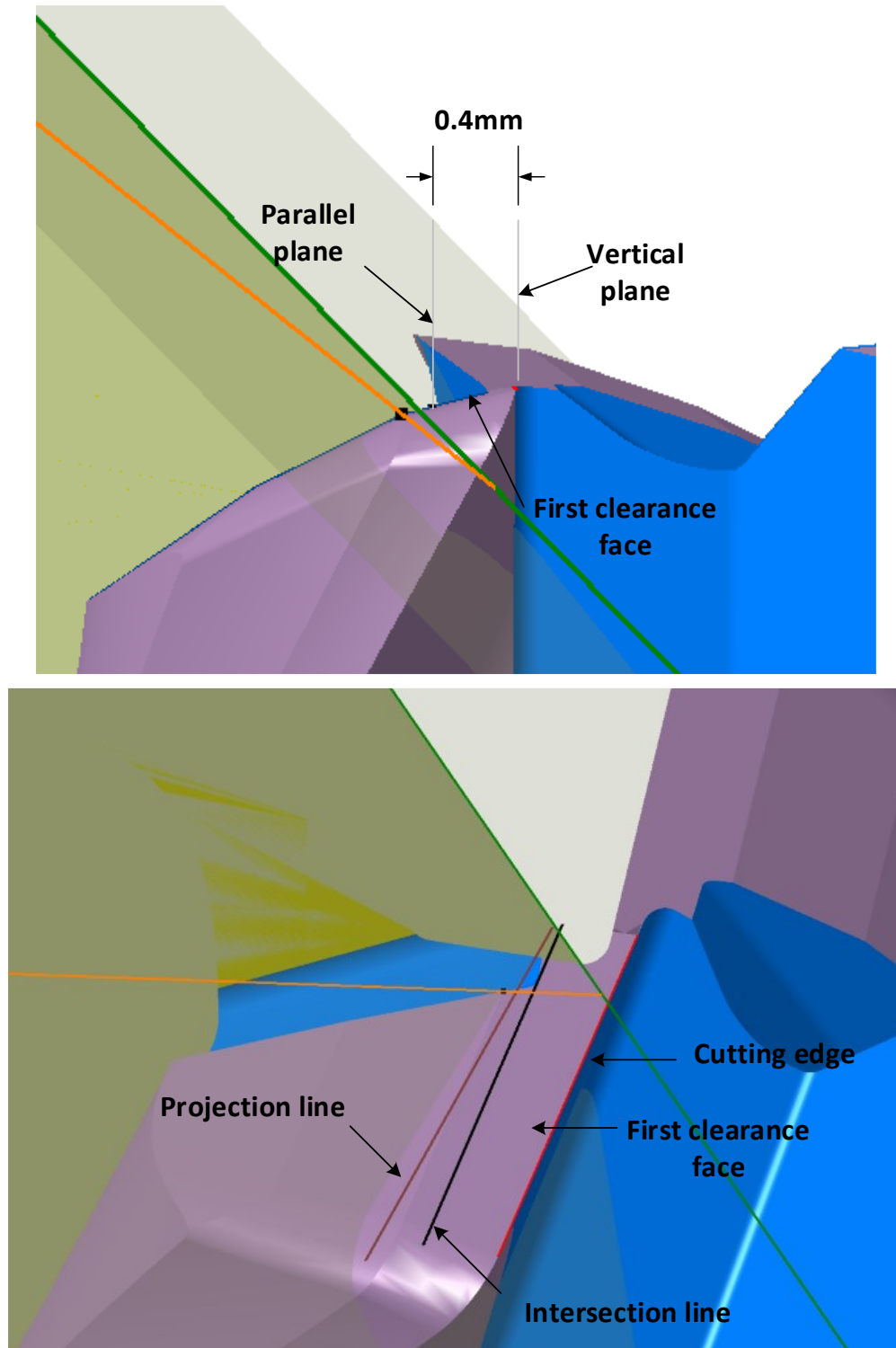


**Figure 3.15 Constraint line of gash bottom**

Assuming the long cutting edge coincides with y-axis, and the direction vector and a point of

intersection line is developed, as shown in Figure 3.14.

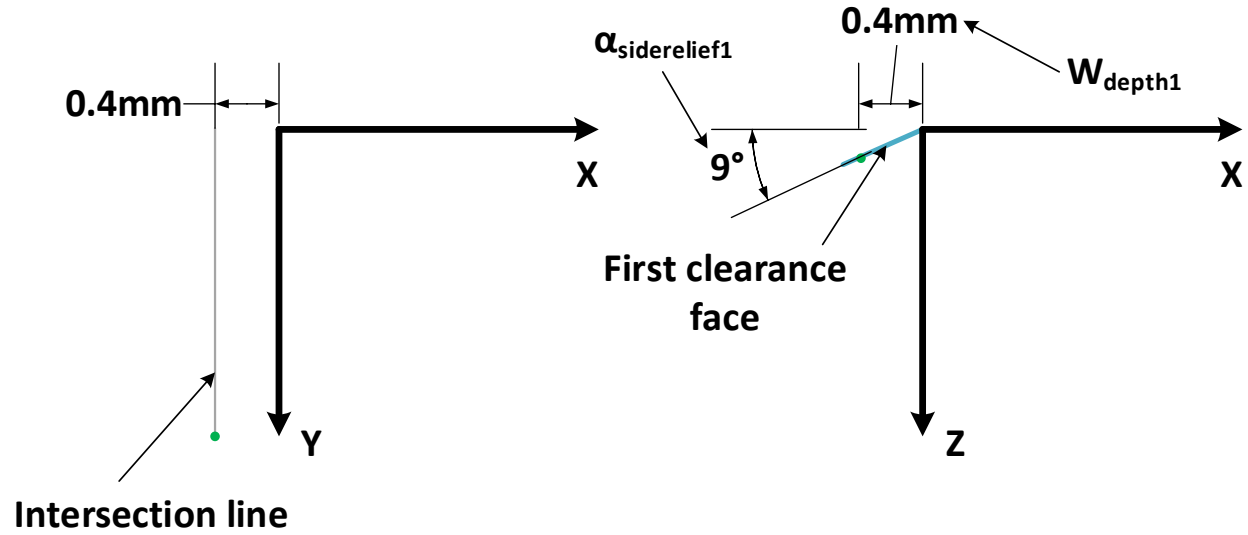


Figure 3.16 Intersection line position

So the coordinate of the green point and the direction vector of intersection line are:

$$P'_{i2} = \begin{bmatrix} -W_{depth1} \\ \frac{D}{2} - R_c \\ W_{depth1} \cdot \tan \alpha_{siderelief1} \end{bmatrix} \quad \text{Eq3.12}$$

$$\vec{d}'_{i2} = \begin{bmatrix} 0 \\ \frac{D}{2} - R_c \\ 0 \end{bmatrix} \quad \text{Eq3.13}$$

Base on the fact that long cutting edge doesn't coincide with y-axis, from Eq2.3, the same transformation matrix is applied:

$$P_{i2} = M_1 M_2 M_3 M_4 M_5 P'_{i2} \quad \text{Eq3.14}$$

$$\vec{d}_{i2} = M_1 M_2 M_3 M_4 M_5 \vec{d}'_{i2} \quad \text{Eq3.15}$$

Where,

$$M_1 = \begin{bmatrix} 1 & 0 & 0 & 0 \\ 0 & 1 & 0 & -\left(\frac{D}{2} - R_c\right) \\ 0 & 0 & 1 & 0 \\ 0 & 0 & 0 & 1 \end{bmatrix}$$

$$M_2 = \begin{bmatrix} 1 & 0 & 0 & 0 \\ 0 & \cos(-\alpha_I) & \sin(-\alpha_I) & 0 \\ 0 & -\sin(-\alpha_I) & \cos(-\alpha_I) & 0 \\ 0 & 0 & 0 & 1 \end{bmatrix}$$

$$M_3 = \begin{bmatrix} \cos \theta & \sin \theta & 0 & 0 \\ -\sin \theta & \cos \theta & 0 & 0 \\ 0 & 0 & 1 & 0 \\ 0 & 0 & 0 & 1 \end{bmatrix}$$

$$M_4 = \begin{bmatrix} 1 & 0 & 0 & 0 \\ 0 & 1 & 0 & \frac{D}{2} - R_c \\ 0 & 0 & 1 & 0 \\ 0 & 0 & 0 & 1 \end{bmatrix}$$

$$M_5 = \begin{bmatrix} \cos(-\theta) & \sin(-\theta) & 0 & 0 \\ -\sin(-\theta) & \cos(-\theta) & 0 & 0 \\ 0 & 0 & 1 & 0 \\ 0 & 0 & 0 & 1 \end{bmatrix}$$

So,

$$P_{i2} = \begin{bmatrix} \sin \theta \cdot \left(\frac{D}{2} - R_c\right) - W_{depth1} \\ \left(\frac{D}{2} - R_c\right) \cdot (\cos \alpha_I - 1 + \cos \alpha_I \cdot \cos \theta) - W_{depth1} \cdot \sin \alpha_I \cdot \tan \alpha_{siderelief1} \\ \left(\frac{D}{2} - R_c\right) \cdot \sin \alpha_I \cdot (\cos \theta + 1) + W_{depth1} \cdot \cos \alpha_I \cdot \tan \alpha_{siderelief1} \end{bmatrix}$$

$$\vec{d}_{i2} = \begin{bmatrix} \sin \theta \cdot \left(\frac{D}{2} - R_c\right) \\ \left(\frac{D}{2} - R_c\right) \cdot (\cos \alpha_I - 1 + \cos \alpha_I \cdot \cos \theta) \\ \left(\frac{D}{2} - R_c\right) \cdot \sin \alpha_I \cdot (\cos \theta + 1) \end{bmatrix}$$

Then the parametric Equation of intersection line is:

$$P_{line2}(t) = \begin{bmatrix} x_{pi2} + x_{di2} \cdot t \\ y_{pi2} + y_{di2} \cdot t \\ z_{pi2} + z_{di2} \cdot t \end{bmatrix} \quad \text{Eq3.16}$$

Where,

$$P_{i2} = \begin{bmatrix} x_{pi2} \\ y_{pi2} \\ z_{pi2} \end{bmatrix}$$

$$\vec{d}_{i2} = \begin{bmatrix} x_{di2} \\ y_{di2} \\ z_{di2} \end{bmatrix}$$

To derive the projection line, as shown in Figure 3.13, the norm vector of plane that passes through intersection line and projection line is developed:

$$\vec{n}_{plane-ip} = \vec{n}_{base} \times \vec{d}_{i2} \quad \text{Eq3.17}$$

Where  $\vec{n}_{base}$  is the norm vector of base plane and  $\vec{d}_{i2}$  is the direction vector of intersection line. The direction vector of projection line is:

$$\vec{d}_{projection} = \vec{n}_{base} \times \vec{n}_{plane-ip} \quad \text{Eq3.18}$$

The intersection point  $P_{i3}$ , which is shared by intersection line and base plane, also lying on projection line, is obtained by solving Equation group of Eq3.16 and Eq3.9. The parametric Equation of projection line is:

$$P_{projection}(t) = \begin{bmatrix} x_{pi3} + x_{dpro} \cdot t \\ y_{pi3} + y_{dpro} \cdot t \\ z_{pi3} + z_{dpro} \cdot t \end{bmatrix} \quad \text{Eq3.19}$$

Where,

$$P_{i3} = \begin{bmatrix} x_{pi3} \\ y_{pi3} \\ z_{pi3} \end{bmatrix}$$

$$\vec{d}_{projection} = \begin{bmatrix} x_{dpro} \\ y_{dpro} \\ z_{dpro} \end{bmatrix}$$

Since the main part of gash profile is developed, the features left are stated and generated as follow: The first circle  $C_1$ , with a radius of  $R_{gashcorner1}$ , is generated by bitangent to the second side

line and the projection line. Similarly, the second circle  $C_2$ , which is tangent to projection line and first side line, is found and the two circles possess the same radius. Using CATIA function, two circles can be generated easily, as shown in Figure 3.15.

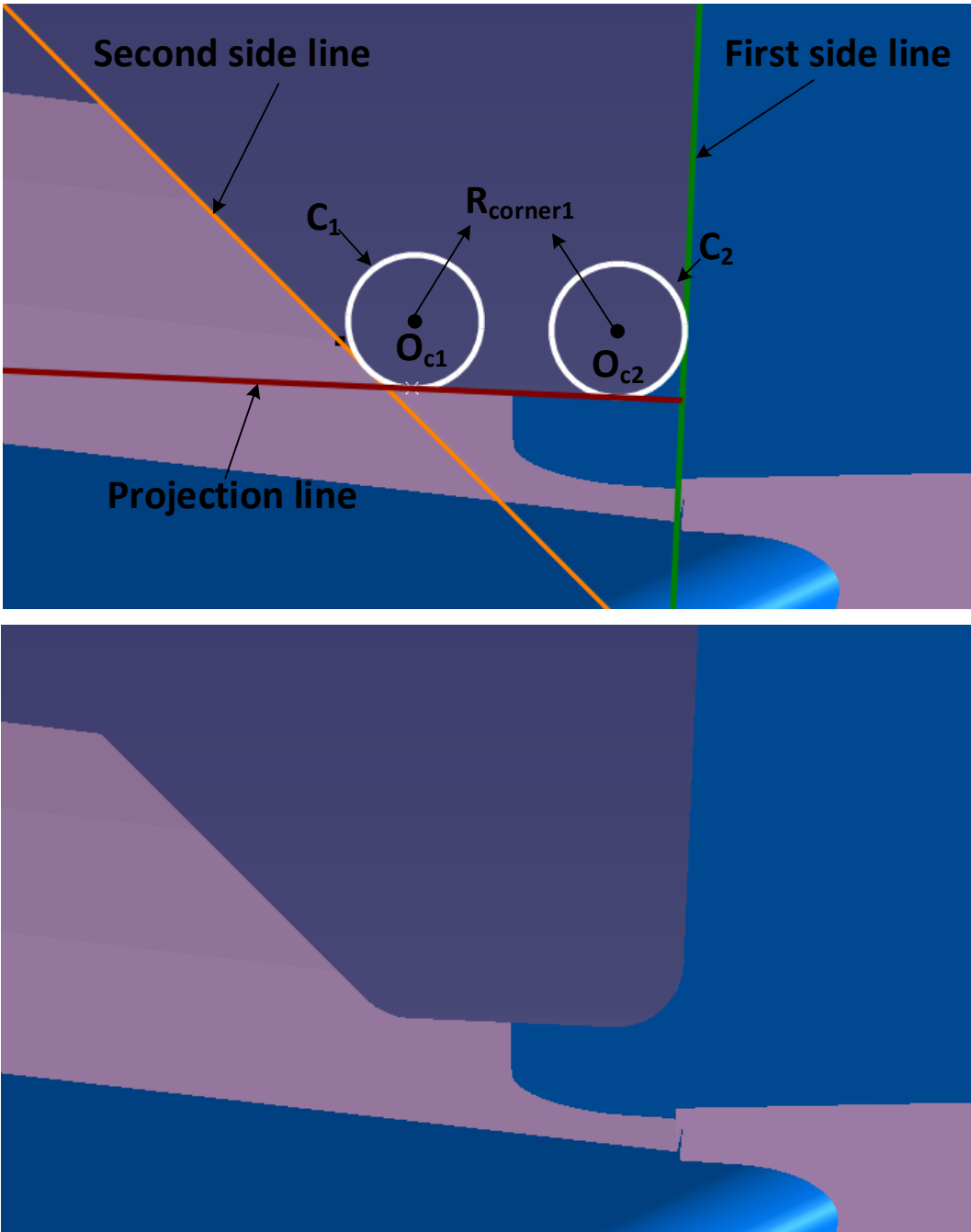
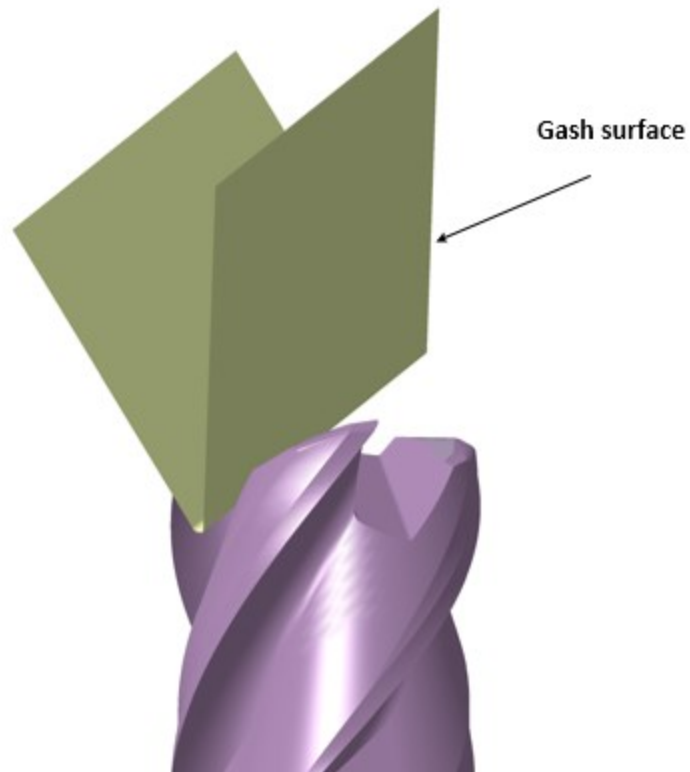


Figure 3.17 Gash profile

With the gash profile developed above, using extrude function in CATIA, a gash surface is derived, shown in Figure 3.15.



**Figure 3.18 Gash surface**

All the features of end-mill are generated, then Boolean operation is utilized to obtain the final model of end-mill, as shown in Figure 3.16.



**Figure 3.19 Final model of end mill**

With all the parametric equations are derived, the feature can be built and the final model is obtained.

# CHAPTER 4 PARAMETRIC MODELING

## PROGRAM OF END MILL

### 4.1 Customized Modeling Program

Based on the fact that end mill cutter has a complicated structure and the modeling procedure of end mill is time consuming, a rapid modeling program is needed. Visual Basic (VB.NET) is a simple and widely used programming language. It is easy to design a user interface on Visual Studio platform. Most importantly, CATIA provides interface for Visual Basic so that the modeling program is feasible.

The customized modeling program is developed as following the procedure. Firstly, a blank VB.NET project is created and all corresponding interfaces of CATIA are added to the project as references. Then, the user interface of modeling program is generated as shown in Figure 4.1. The model is divided into features and each tab contains the design parameters of the feature. Finally, the modeling code is written into a function module and the module is added to the project. The model is built feature by feature as mentioned before.

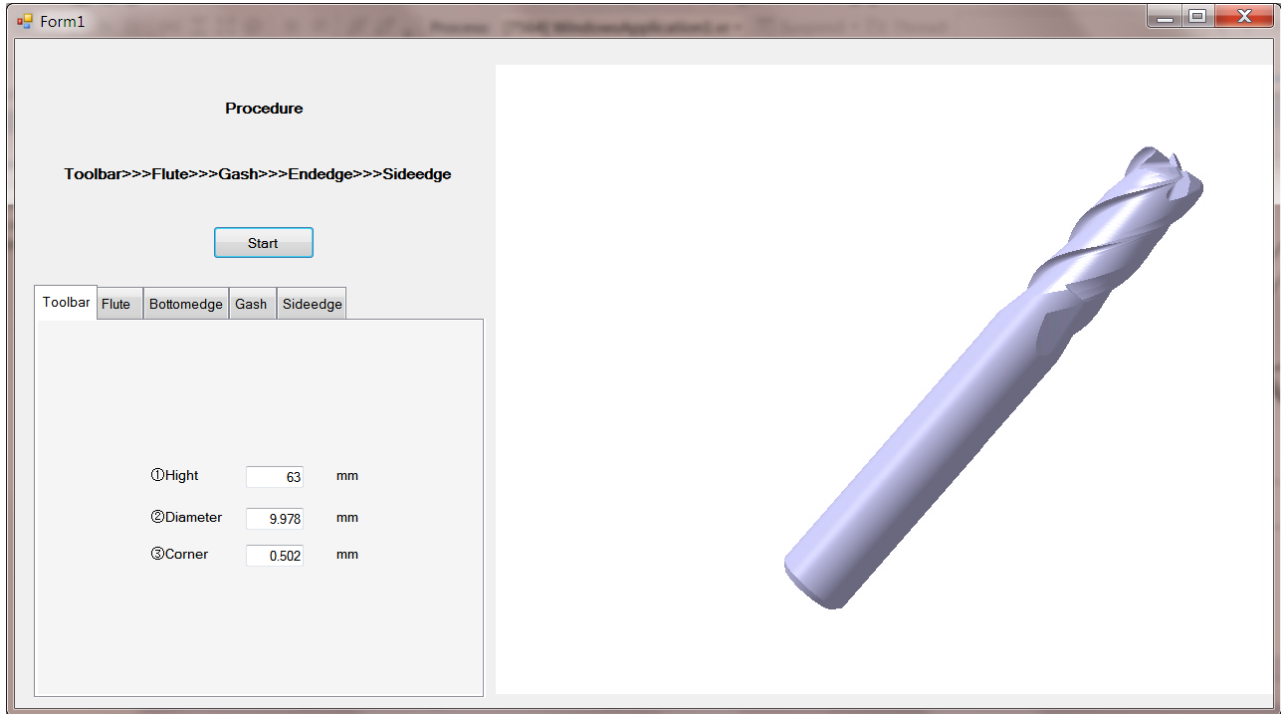


Figure 4.1 User face of program

## 4.2 Verification of the Modeling Program

To prove the reliability and accuracy of the program, a set of parameters is measured from a real end mill cutter. This set of parameters is used to build the end mill cutter model to verify the reliability. The model is also measured in CATIA to check the accuracy. The measured parameters are shown in Table 4.1.

Table 4.1 Parameters of cutter STR440M

Tab Name	Parameter Name	Value
toolbar	L	63mm
	D	9.978mm

	$R_c$	0.502mm
<b>Flute</b>		
1	$\alpha_{fluteangle1}$	81.5°
	$L_{flutlength1}$	13.5mm
	$\beta_{helix1}$	41°
2	$\alpha_{fluteangle2}$	92.5°
	$L_{flutlength2}$	13.5mm
	$\beta_{helix2}$	38°
3	$\alpha_{fluteangle3}$	85.5°
	$L_{flutlength3}$	13.5mm
	$\beta_{helix3}$	41°
4	$\alpha_{fluteangle4}$	100.5°
	$L_{flutlength4}$	13.5mm
	$\beta_{helix4}$	38°
<b>Bottom edge</b>		
1	$\alpha_{l1}$	1.8°
	$D_{radialoffset1}$	0
	$D_{axialoffset1}$	2.42mm
	$\alpha_{rake1}$	5.5°
	$\alpha_{relief11}$	10°
	$\alpha_{relief12}$	24°

	$\alpha_{\text{relief13}}$	30°
	$W_{\text{relief11}}$	0.85mm
	$W_{\text{relief12}}$	1.2mm
	$W_{\text{relief13}}$	3mm
2	$\alpha_{\text{i2}}$	1.8°
	$D_{\text{radialoffset2}}$	0.1mm
	$D_{\text{axialoffset2}}$	0
	$\alpha_{\text{rake2}}$	5.5°
	$\alpha_{\text{relief21}}$	10°
	$\alpha_{\text{relief22}}$	24°
	$\alpha_{\text{relief23}}$	30°
	$W_{\text{relief21}}$	0.85mm
	$W_{\text{relief22}}$	1.2mm
	$W_{\text{relief23}}$	3mm
3	$\alpha_{\text{i3}}$	1.8°
	$D_{\text{radialoffset3}}$	0
	$D_{\text{axialoffset3}}$	2.42mm
	$\alpha_{\text{rake3}}$	5.5°
	$\alpha_{\text{relief31}}$	10°
	$\alpha_{\text{relief32}}$	24°
	$\alpha_{\text{relief33}}$	30°
$W_{\text{relief31}}$	0.85mm	

	$W_{\text{relief32}}$	1.2mm	
	$W_{\text{relief33}}$	3mm	
	$\alpha_{l4}$	1.8°	
	$D_{\text{radialoffset4}}$	0.1mm	
	$D_{\text{axialoffset4}}$	0	
	$\alpha_{\text{rake4}}$	5.5°	
4	$\alpha_{\text{relief41}}$	10°	
	$\alpha_{\text{relief42}}$	24°	
	$\alpha_{\text{relief43}}$	30°	
	$W_{\text{relief41}}$	0.85mm	
	$W_{\text{relief42}}$	1.2mm	
	$W_{\text{relief43}}$	3mm	
	<b>Side edge</b>		
	1	$\alpha_{\text{siderelief11}}$	9°
		$\alpha_{\text{siderelief12}}$	25°
$\alpha_{\text{siderelief13}}$		30°	
$W_{\text{siderelief11}}$		0.6mm	
$W_{\text{siderelief12}}$		1.2mm	
$W_{\text{siderelief13}}$		3mm	
2	$\alpha_{\text{siderelief21}}$	9°	
	$\alpha_{\text{siderelief22}}$	25°	

	$\alpha_{\text{siderelief23}}$	30°
	$W_{\text{siderelief21}}$	0.6mm
	$W_{\text{siderelief22}}$	1.2mm
	$W_{\text{siderelief23}}$	3mm
3	$\alpha_{\text{siderelief31}}$	9°
	$\alpha_{\text{siderelief32}}$	25°
	$\alpha_{\text{siderelief33}}$	30°
	$W_{\text{siderelief31}}$	0.6mm
	$W_{\text{siderelief32}}$	1.2mm
	$W_{\text{siderelief33}}$	3mm
	4	$\alpha_{\text{siderelief41}}$
$\alpha_{\text{siderelief42}}$		25°
$\alpha_{\text{siderelief43}}$		30°
$W_{\text{siderelief41}}$		0.6mm
$W_{\text{siderelief42}}$		1.2mm
$W_{\text{siderelief43}}$		3mm
<b>Gash</b>		
1	$W_{\text{depth1}}$	0.4mm
	$W_{\text{width1}}$	1mm
	$R_{\text{gashcorner1}}$	0.2mm
	$\alpha_{\text{guide1}}$	38°

	$\alpha_{\text{gash1open}}$	$47^\circ$
	$\alpha_{\text{gash1bottm}}$	$90^\circ$
2	$W_{\text{depth2}}$	0.5mm
	$W_{\text{width4}}$	1mm
	$R_{\text{gashcorner2}}$	0.2mm
	$\alpha_{\text{guide2}}$	$38^\circ$
	$\alpha_{\text{gash2open}}$	$47^\circ$
	$\alpha_{\text{gash2bottm}}$	$120^\circ$
	3	$W_{\text{depth3}}$
$W_{\text{width3}}$		1mm
$R_{\text{gashcorner3}}$		0.2mm
$\alpha_{\text{guide3}}$		$38^\circ$
$\alpha_{\text{gash3open}}$		$47^\circ$
$\alpha_{\text{gash3bottm}}$		$90^\circ$
4		$W_{\text{depth4}}$
	$W_{\text{width4}}$	1mm
	$R_{\text{gashcorner4}}$	0.2mm
	$\alpha_{\text{guide4}}$	$38^\circ$
	$\alpha_{\text{gash4open}}$	$47^\circ$
	$\alpha_{\text{gash4bottm}}$	$120^\circ$

With the parameters above, the model of end mill cutter is developed in CATIA by using the

program. The parameters of the model are measured in CATIA, as shown in Figure 4.2 to Figure 4.6 below. The measured parameters indicate the precision of the model and the analysis of the model does make sense.

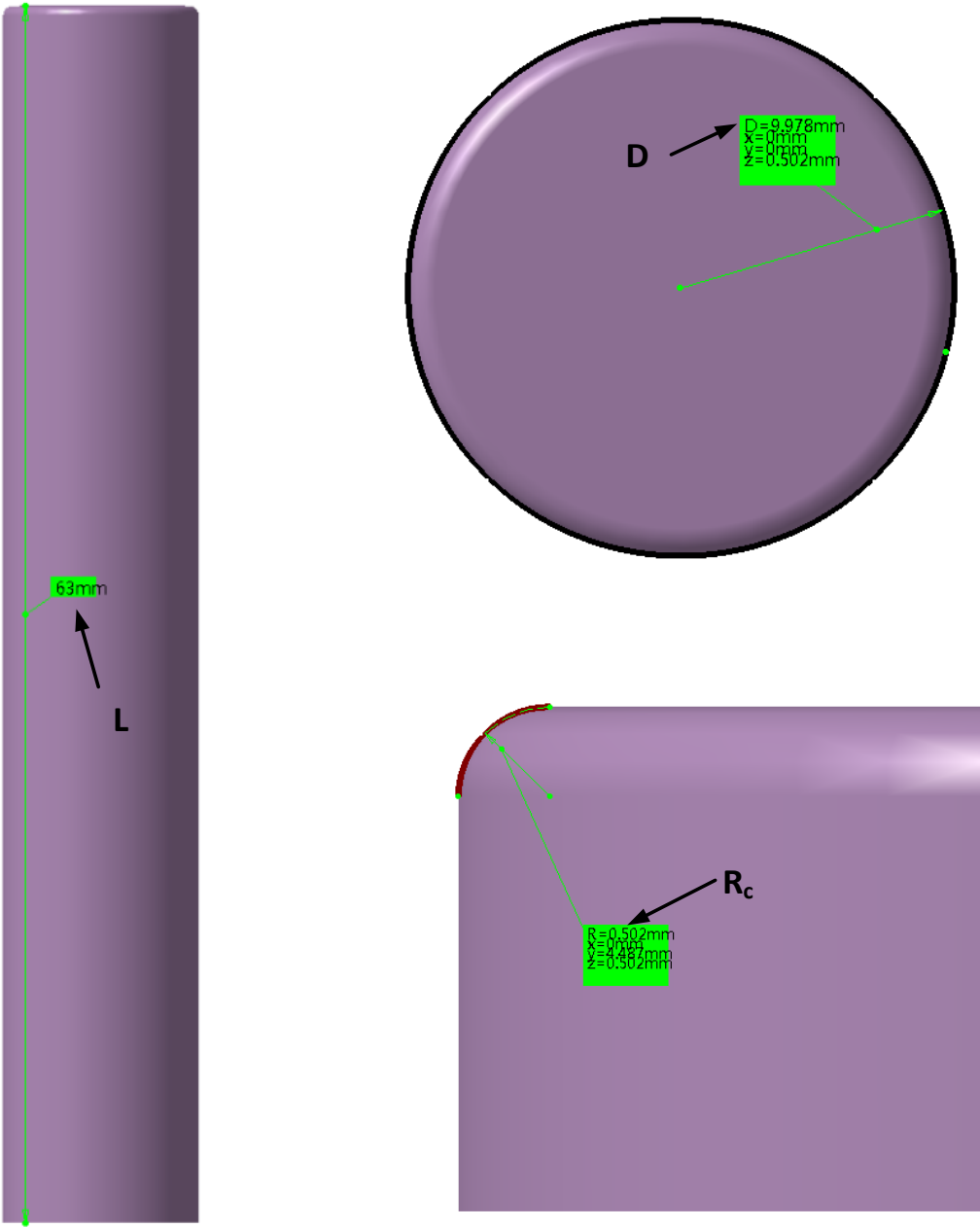


Figure 4.2 Toolbar parameters

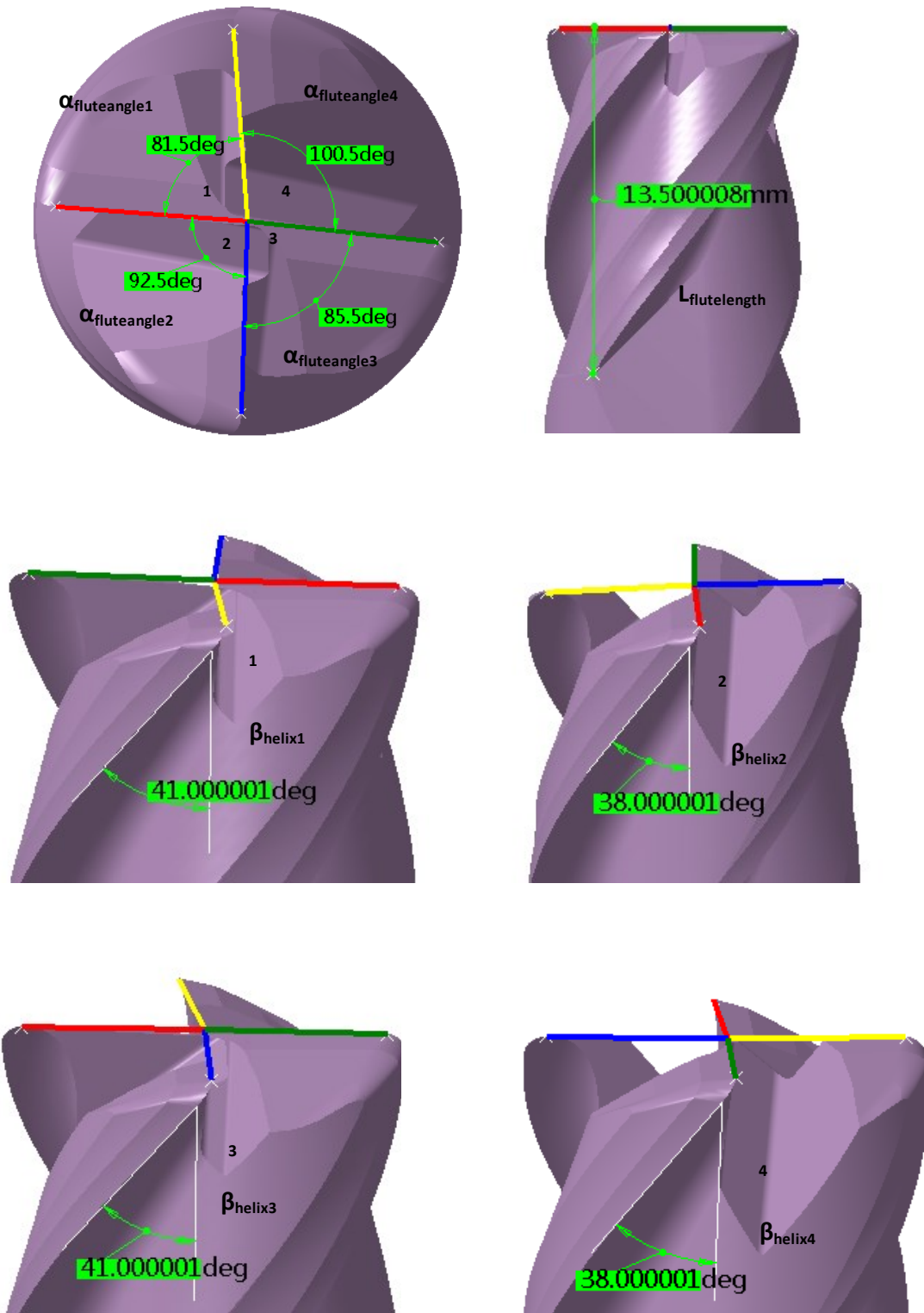


Figure 4.3 Flute parameters

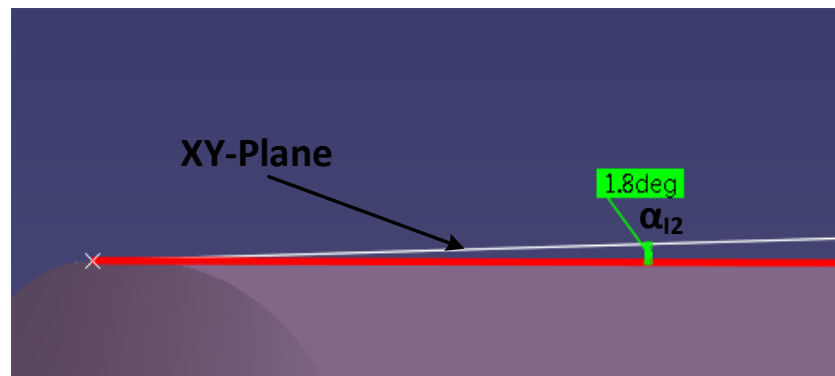
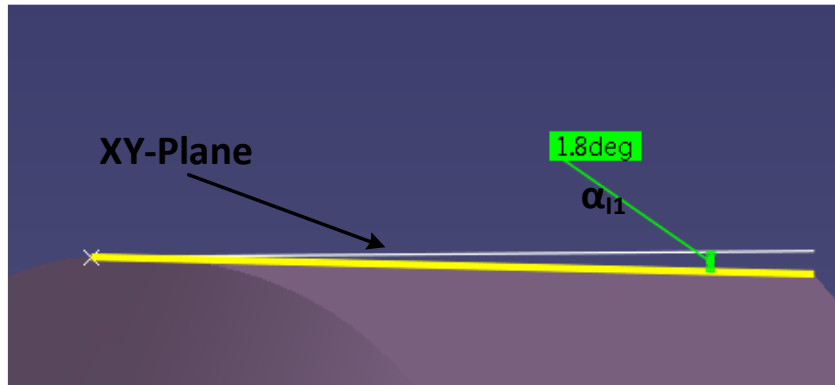
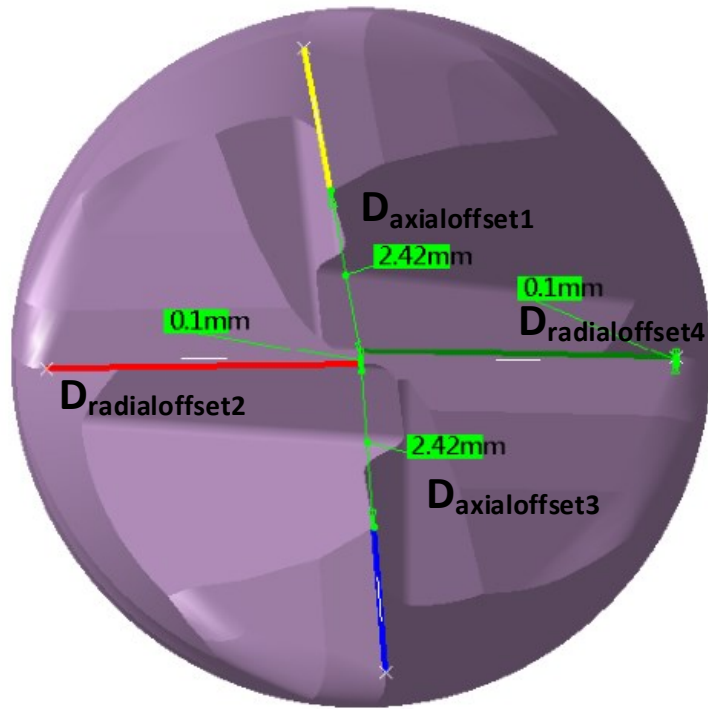
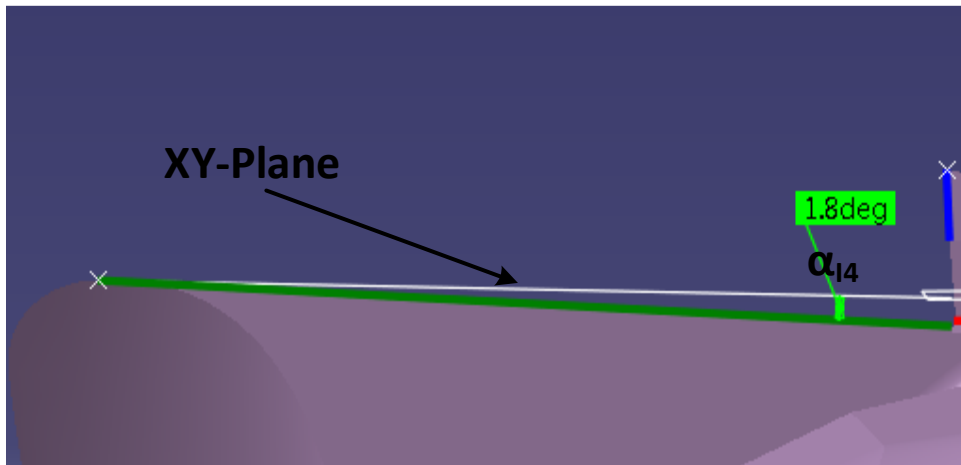
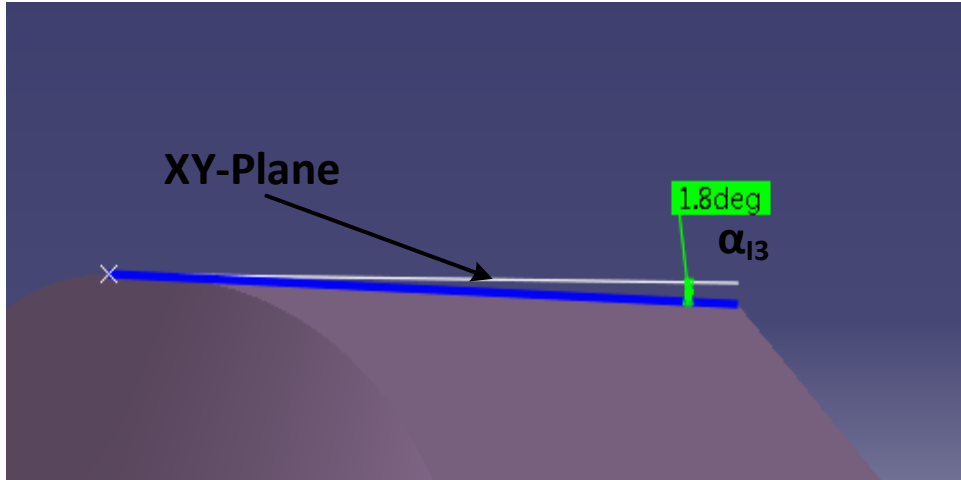
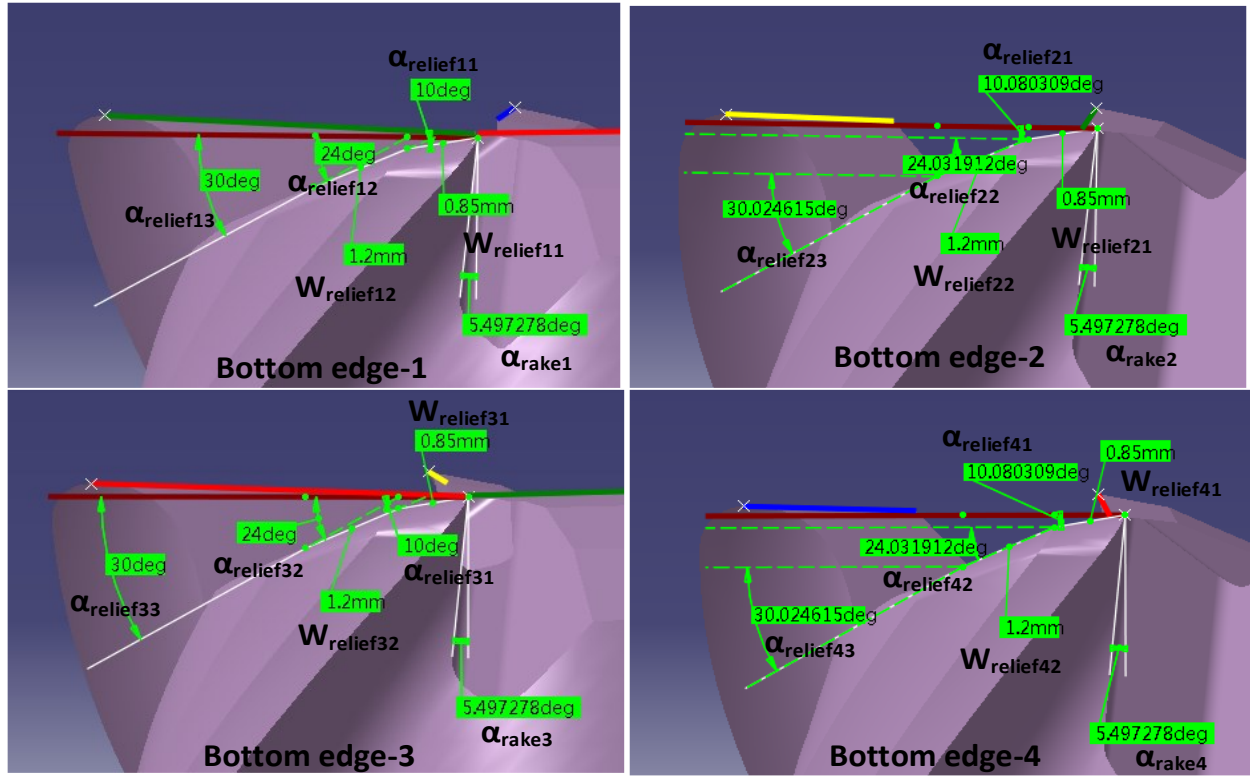


Figure 4.4 Bottom edge parameters



Continue of Figure 4.4



Continue of Figure 4.4

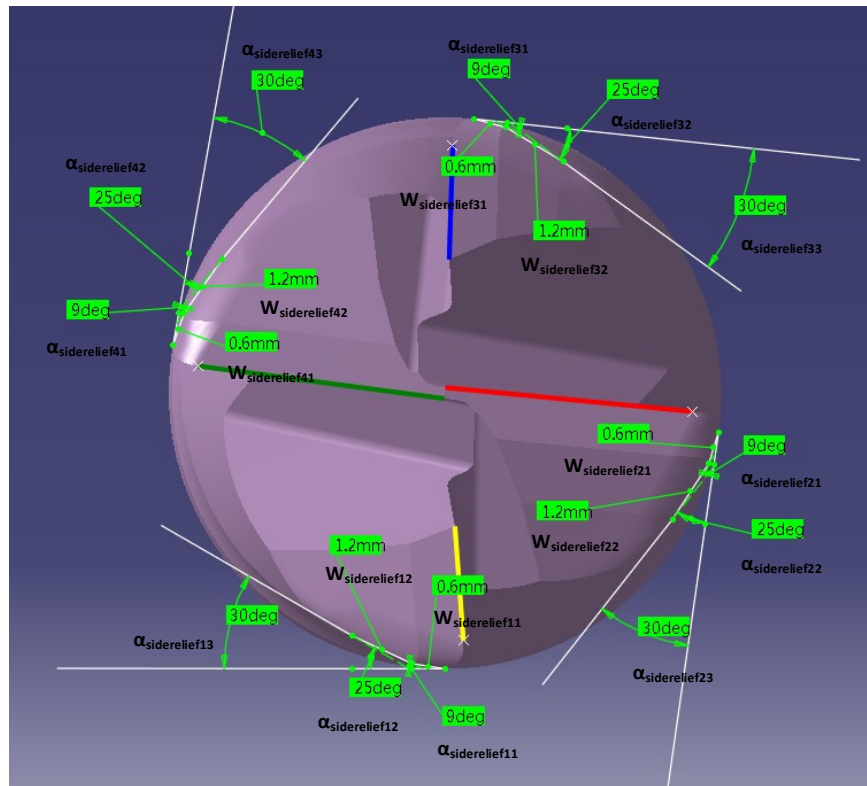


Figure 4.5 Side edge parameters

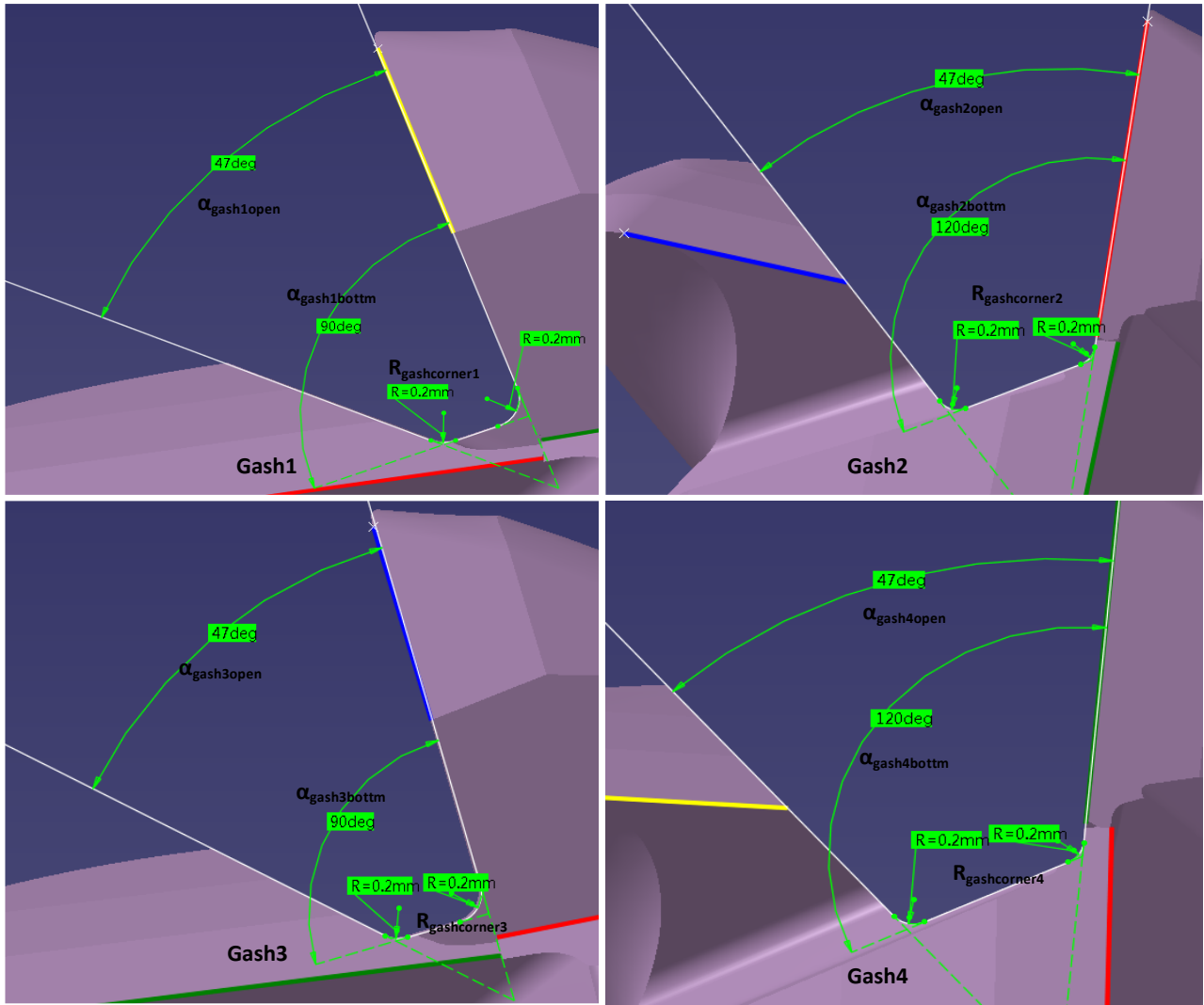
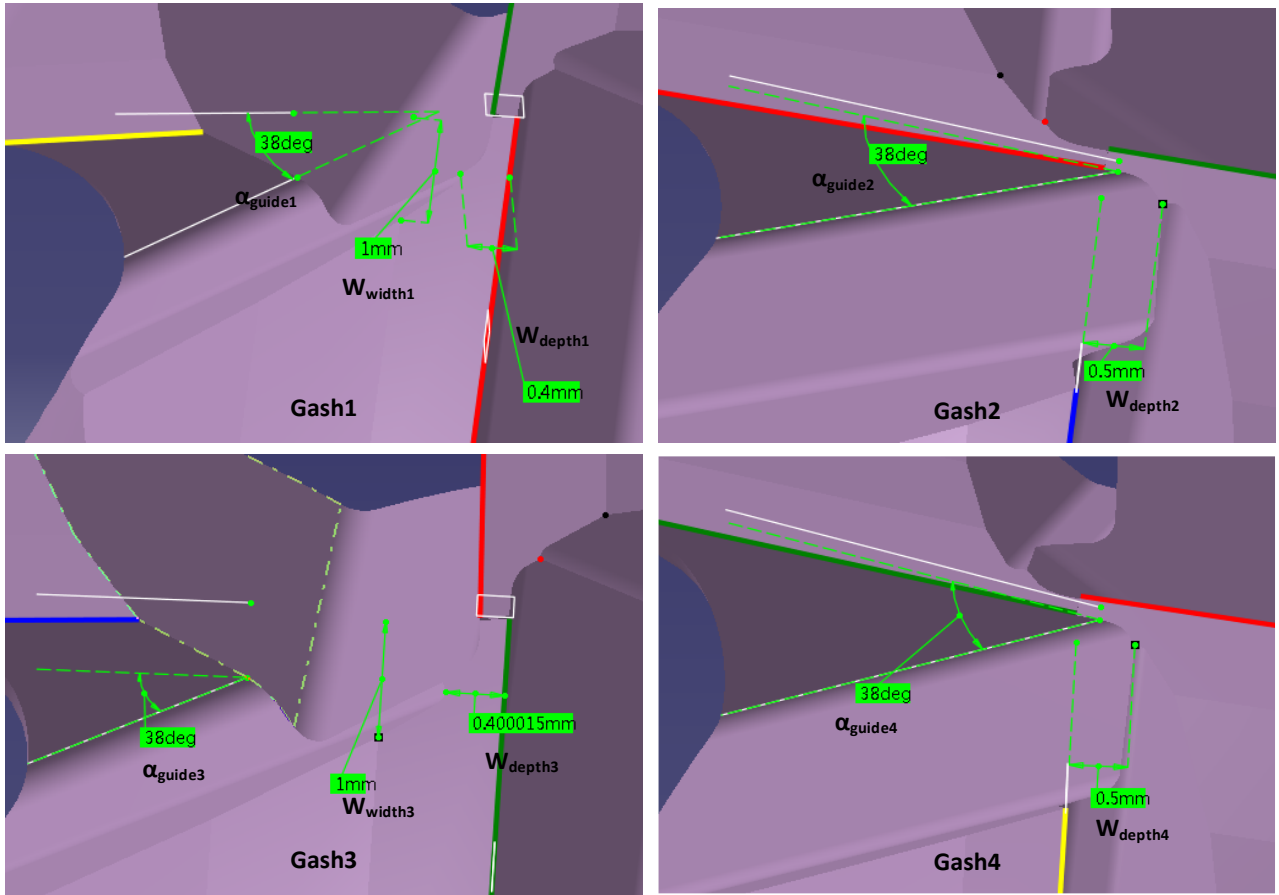


Figure 4.6 Gash parameters



Continue of Figure 4.6

# CHAPTER 5 APPLICATION

## 5.1 Introduction

Generally, after the end mill cutter is designed, it will be machined by grinding wheel. Then, the dynamics of the cutter is explored through experiments to decide if the requirement is satisfied. However, this process is time consuming and costly. Since the end mill cutter can be built using the modeling program, FEA is introduced to simulate the cutting process and the cutting dynamics is measured. The dynamics can be treat as a guide to optimize the design of end mill cutter.

Third Wave Advantedge is a famous software for optimization of metal cutting with validated finite element technique to simulate machining processes in 2D and 3D environments. The end mill model can be imported into Third Wave for further analysis. By setting up the parameters of the cutting process, the result of cutting process is deduced by this software and the simulated cutting dynamics is obtained, such as: temperature, stress, chip formation and power consumption.

## 5.2 Settings of Simulation Software

The first step of simulation process is the project setting. To start the simulation process, a new project is created first and the process type is selected as well, as shown in Figure5.1.

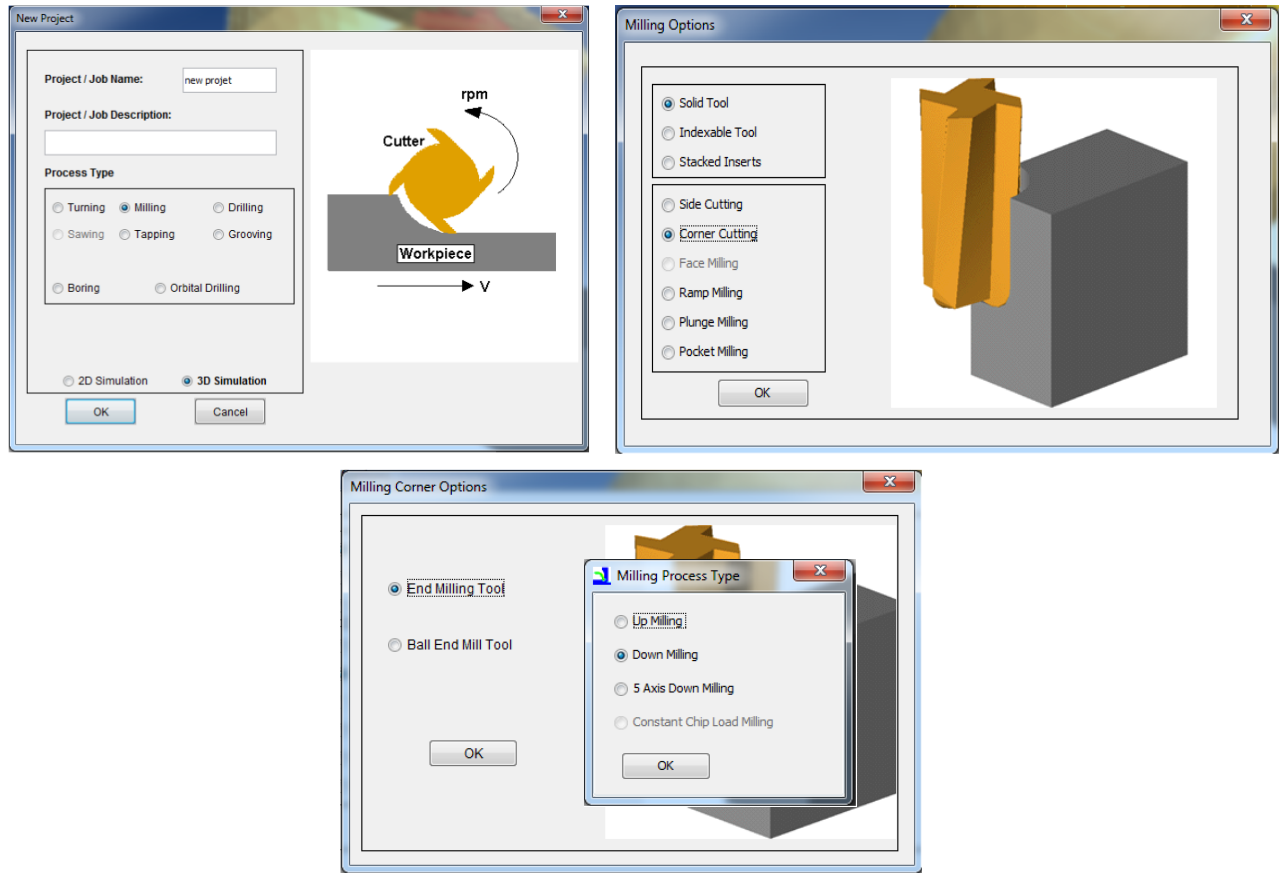


**Figure 5.1 Project setting**

The second step is to set up the parameters about cutting tool and work piece. The cutting tool model is imported to the software and the mesh parameters should be determined. In this case, the bottom part of the end mill cutter is imported and the dynamics of the corner are derived. After that a standard work piece is generated and the mesh parameters of work piece are defined, as shown in Figure 5.2.

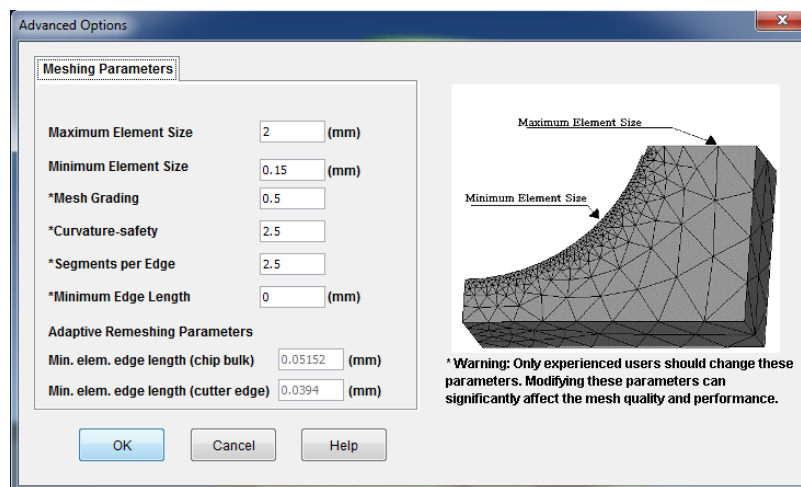
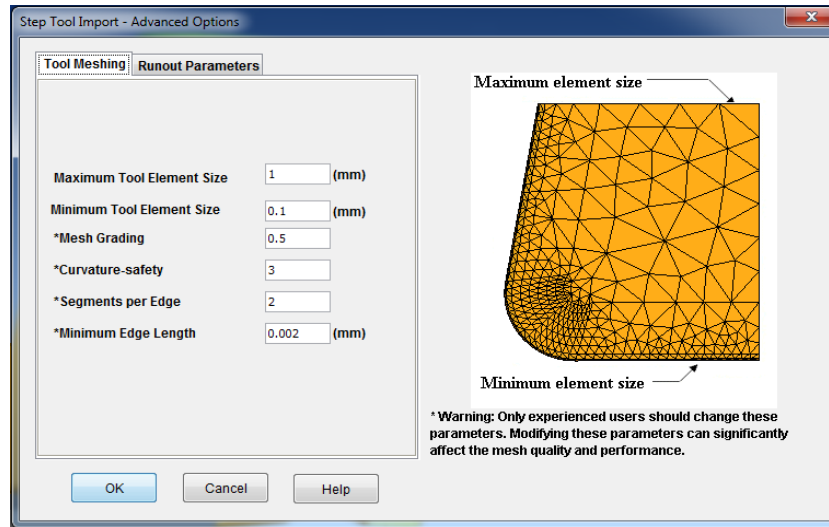
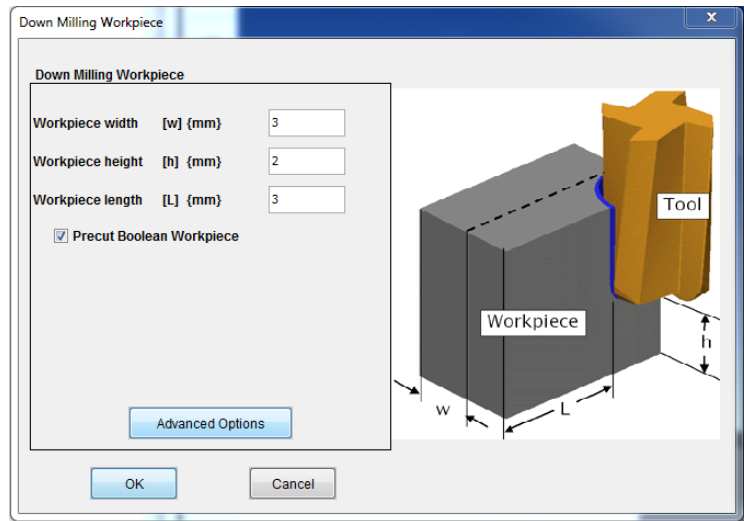
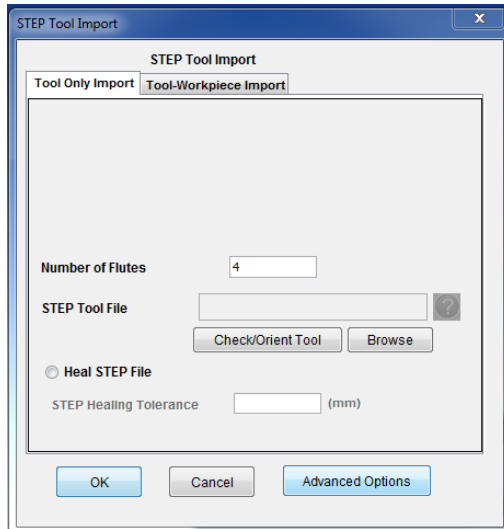


**Figure 5.2 Cutting tool and work piece setting**

The third step is to select the material for the cutter and work piece. In this case, a typical

nickel-based high temperature, Inconel718, is chosen as the work piece material and a general cutting tool material, Carbide-Grade-K, is taken as the end mill cutter material. Then the simulation model is redrawn, as shown in Figure5.3.

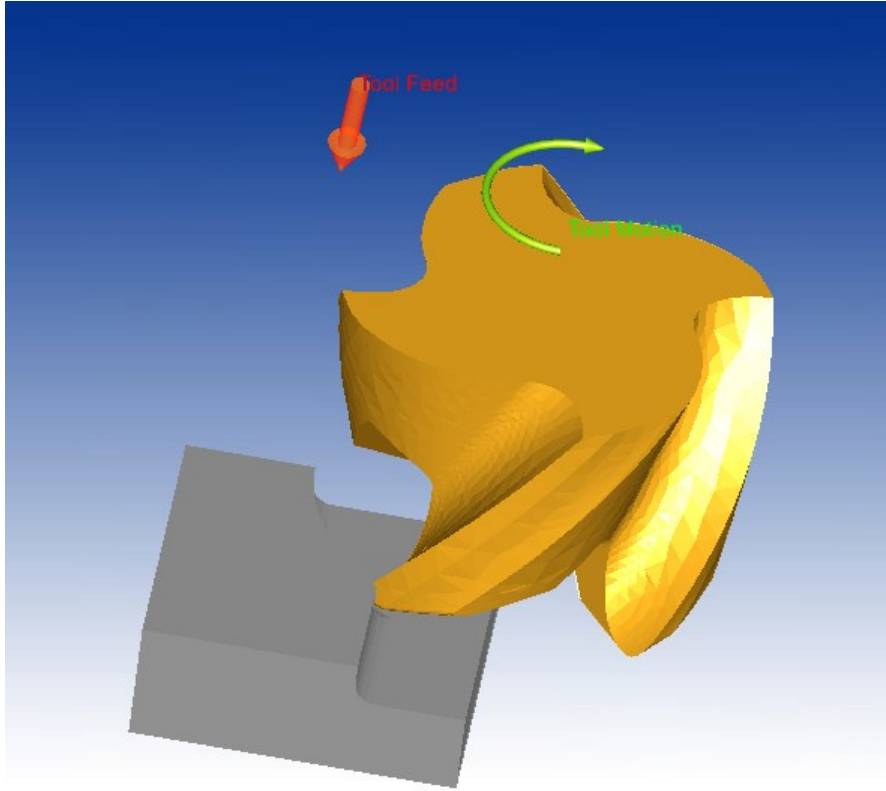


**Figure 5.3 Redrawn model**

Finally, the parameters of cutting process, which include feed rate, spindle speed, radial width of cut, axial depth of cut, initial temperature and angle of rotation, are determined, as shown in Figure 5.4.

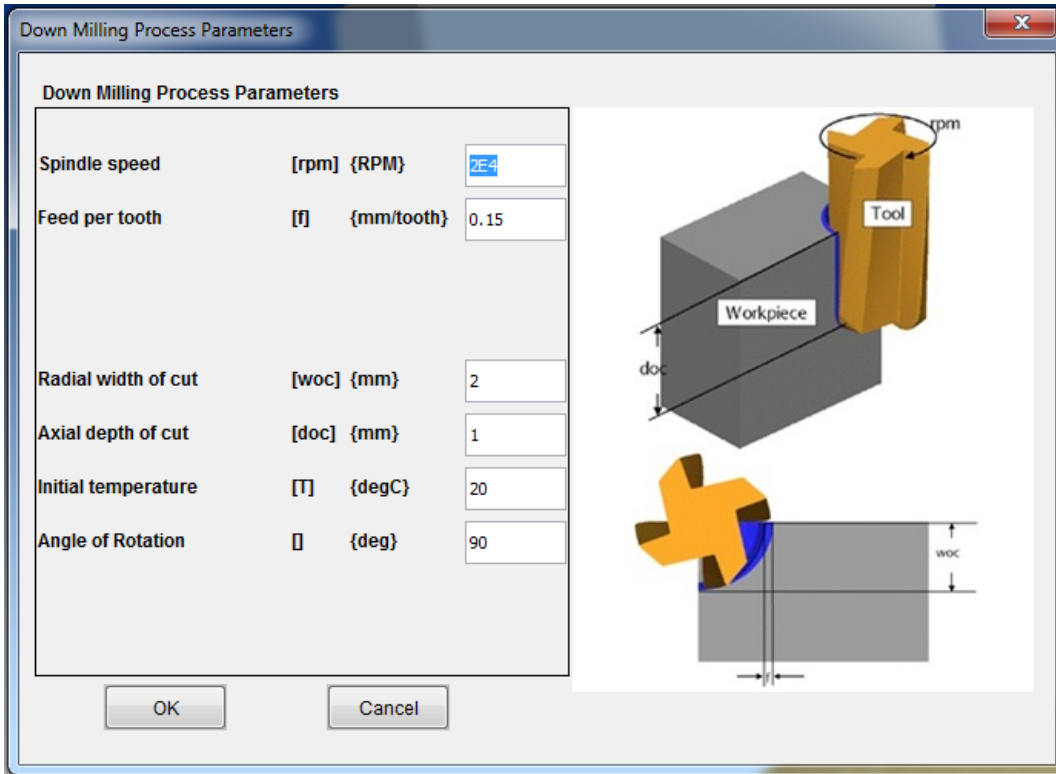


**Figure 5.4 Parameters of cutting process**

After all parameters is set up, the project is calculated. The simulation result is shown is Figure 5.5. The range of cutting force along each axis is derived and the temperature during cutting displayed in different colors. The highest temperature is reached as well. By modifying design parameters, the simulation result will change. The simulation result could match the design requirement with the adjustment of design parameters and final cutting tool model is developed.

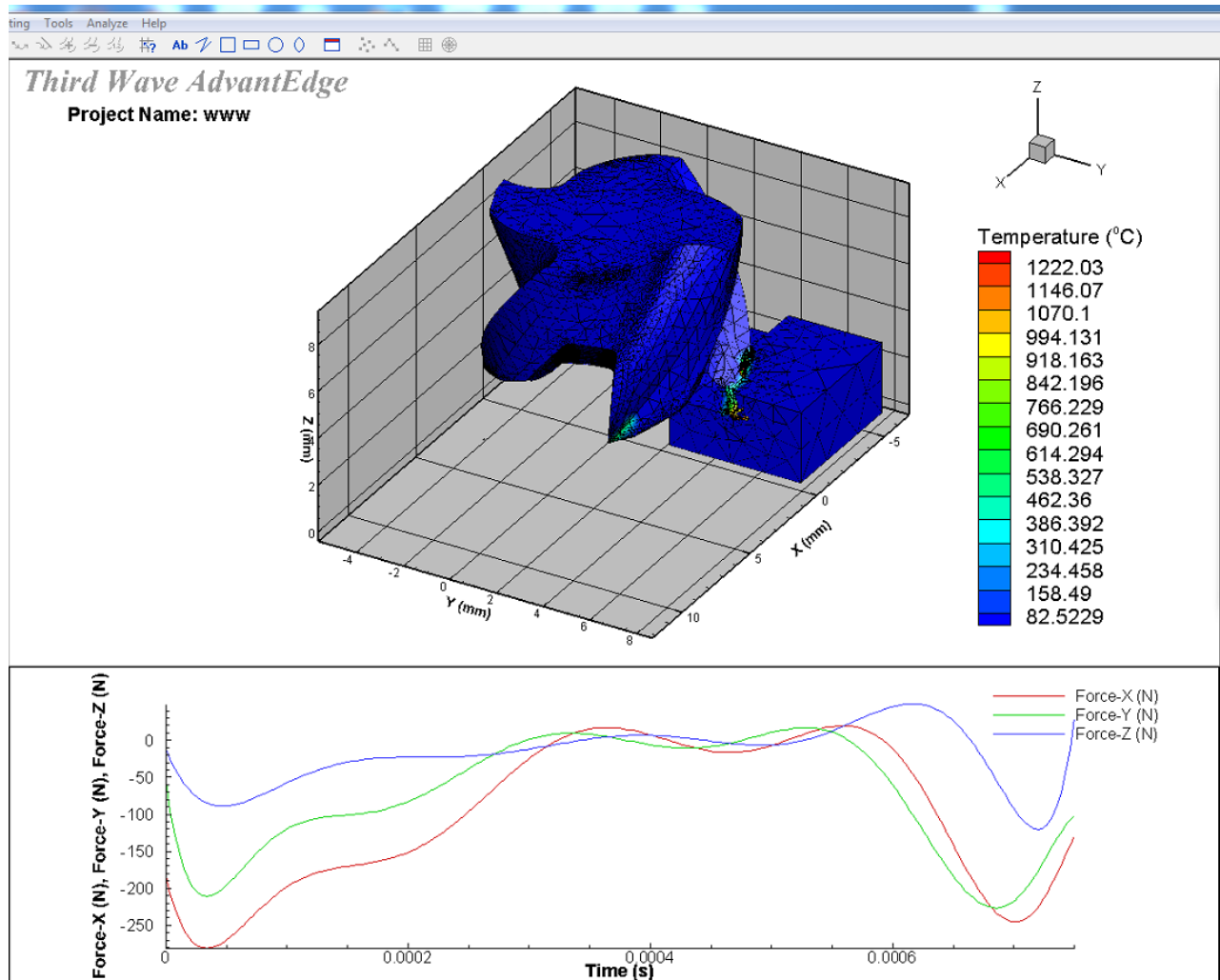


Figure 5.5 Simulation result

# CHAPTER 6 CONCLUSIONS AND FUTURE WORK

## 6.1 Conclusions

In this thesis, an integrated feature-based modeling method is proposed. With the combination of Visual Basic interface and CATIA macro programming technique, a customized feature-based modeling program is developed.

For flute modeling, an accurate flute profile model is used. According to the parametric Equation, the points on the flute profile are calculated with MATLAB. By inputting the data of points, flute profile is reached. With the function of sweep surface, the flute is generated by sweeping the flute profile along the corresponding helix line.

In cutting edge part, with constraints, the position of cutting edge is found according to the Equation and the exterior endpoint is reached. Then orthogonal cutting model is introduced. By applying this theory, cutting edge profile is developed on the orthogonal plane. Sweep surface function is used to build the clearance face of bottom cutting edge and side cutting edge. Since there is no theory and design parameters about fillet, based on the position of clearance of bottom and side, fill surface is utilized to build a smooth fillet relief. Meanwhile, the fillet edge is ensured.

The machining process of gash is discussed first. Then, an accurate gash model is introduced. With the given design parameters, guide direction line is found and gash profile is fixed. At last, sweep surface function is applied to develop the final gash face.

With the combination of Visual Basic and CATIA macro programming technique, a customized modeling program, which is based on end-mill feature, is derived. A simple model, built with measured parameters, is formed using the parametric program. Finally, a FEA simulation is conducted and the result is used as a guide for optimization of the cutting tool design.

## **6.2 Future Work**

For future research, several topics are considered to expand the present research work.

In this thesis, fillet clearance face is smooth enough to meet the demand. However, research could be done on the fillet clearance face and mathematic model could be built. Meanwhile, a standard rake of fillet is applied in this thesis, but customized rake face of fillet is more and more popular which reinforce the strength of the fillet and lead to a longer life.

This thesis focus on commonly four flutes end mill. Multi-flute end mill has its advantage in some particular situation. Research on this part could enrich the function of the parametric program.

# BIBLIOGRAPHY

1. Salomons, Otto W., Fred JAM van Houten, and H. J. J. Kals. "Review of research in feature-based design." *Journal of Manufacturing Systems* 12.2 (1993): 113-132.
2. Tandon, Puneet, and Md Rajik Khan. "Three dimensional modeling and finite element simulation of a generic end mill." *Computer-Aided Design* 41.2 (2009): 106-114.
3. Kim, Jae Hyun, Jung Whan Park, and Tae Jo Ko. "End mill design and machining via cutting simulation." *Computer-Aided Design* 40.3 (2008): 324-333.
4. Xu, Zhi-Gang, and Bang Zhao. "Research on the design and management of carbide end mill." *SICE-ICASE, 2006. International Joint Conference*. IEEE, 2006.
5. Ren, Bing-Yin, and Yu-Yong Tang. "The general geometrical models of the design and 2-axis NC machining of a helical end-mill with constant pitch." *Journal of Materials Processing Technology* 115.3 (2001): 265-270.
6. Pham, Trung Thanh, and Sung Lim Ko. "A manufacturing model of an end mill using a five-axis CNC grinding machine." *The International Journal of Advanced Manufacturing Technology* 48.5-8 (2010): 461-472.
7. Engin, S., and Y. Altintas. "Mechanics and dynamics of general milling cutters.: Part I: helical end mills." *International Journal of Machine Tools and Manufacture* 41.15 (2001): 2195-2212.

8. Altıntaş, Y., Serafettin Engin, and Erhan Budak. "Analytical stability prediction and design of variable pitch cutters." *Journal of Manufacturing Science and Engineering* 121.2 (1999): 173-178.
9. Zhao, Cai Xia, et al. "A Novel CNC Grinding Method about Relief Surface of Corner Radius End Mill Based on a CAM System." *Applied Mechanics and Materials*. Vol. 120. 2012.
10. Xianfeng, Zhao, Shi Hongyan, and He Lin. "The Mathematic Equation of End mill's Rake Face Based on the Fillet and Two Attitude Angles of Grinding Wheel." *Materials Science Forum*. 2014.
11. Özel, Tuğrul, and Taylan Altan. "Process simulation using finite element method—prediction of cutting forces, tool stresses and temperatures in high-speed flat end milling." *International Journal of Machine Tools and Manufacture* 40.5 (2000): 713-738.
12. Wang, Liming, et al. "A novel approach to determination of wheel position and orientation for five-axis CNC flute grinding of end mills." *The International Journal of Advanced Manufacturing Technology* (2015): 1-16.
13. Kaldor, So, Ada Mod Rafael, and D. Messinger. "On the CAD of profiles for cutters and helical flutes-geometrical aspects." *CIRP Annals-Manufacturing Technology* 37.1 (1988): 53-56.
14. Ehmann, K. F., and M. F. DeVries. "Grinding wheel profile definition for the manufacture of drill flutes." *CIRP Annals-Manufacturing Technology* 39.1 (1990): 153-156.
15. Kang, S. K., K. F. Ehmann, and C. Lin. "A CAD approach to helical groove machining—I. mathematical model and model solution." *International Journal of Machine Tools and Manufacture* 36.1 (1996): 141-153.

16. Kang, S. K., K. F. Ehmann, and C. Lin. "A CAD approach to helical groove machining. Part 2: Numerical evaluation and sensitivity analysis." *International Journal of Machine Tools and Manufacture* 37.1 (1997): 101-117.
  
17. Kim, Yong-Hyun, and Sung-Lim Ko. "Development of design and manufacturing technology for end mills in machining hardened steel." *Journal of materials processing technology* 130 (2002): 653-661.